doi: 10.13133/2280-6148/19085 *Journal of Mediterranean Earth Sciences 17 (2025), 1-26*

J M E S **Journal of Mediterranean Earth Sciences**

Linking sand composition and sequence stratigraphy: insights from the Late Lower Pleistocene to Holocene deposits of the Roman Basin (Latium, central Italy)

Daniel Tentori [1], Salvatore Milli [2,1,*]

[1] *CNR-IGAG, Istituto di Geologia Ambientale e Geoingegneria, Area della Ricerca Roma 1, Roma, Italy*
[2] *Dipartimento di Scienze della Terra, SAPIENZA Università di Roma, Roma, Italy*
**Corresponding author: salvatore.milliu@uniroma1.it*

ABSTRACT - Sand petrographic changes record the interplay between allogenic (e.g., eustatic, climatic, tectonic) and autogenic (e.g., transport, hydraulic sorting, post-depositional alteration) processes that also govern sequence-stratigraphic architecture. The consequence is that compositional trends vary within the systems tract that forms the framework of the high- and low-rank depositional sequences constituting the late Quaternary successions of the Roman basin, a basin supplied by the Tiber River throughout the Pleistocene. The relationship between sediment supply and sediment composition is well evidenced in the Late Lower Pleistocene to Holocene deposits of the high-rank Ponte Galeria Sequence (PGS). This sequence fed by the Tiber River and its tributaries records the dramatic change in sediment composition caused by the introduction of pyroclastic and volcaniclastic material derived by the Pleistocene volcanic complexes of the Roman Magmatic Province. Three main petrofacies (A-C) were recognized in the PGS that have a strong correspondence with the lowstand (LST), transgressive (TST), and highstand (HST) system tracts deposits of the PGS. Petrofacies A (feldspatho-litho-quartzose to feldspatho-quartzo-lithic) reflects erosion of carbonate and siliciclastic sources with minimal volcanic input during LST. Petrofacies B (feldspathic to litho-feldspathic/feldspatho-quartzo-lithic) captures the abrupt volcaniclastic pulse and recycling associated with Pleistocene volcanism during TST. Petrofacies C (feldspatho-quartzo-lithic) best records downstream reworking and Tiber river-mouth processes during HST. In particular, in the modern highstand, upstream sands show a siliciclastic lithic signature, whereas downstream sands are enriched in carbonate and volcanic lithics; coastal hydrodynamics partition detritus into two populations, concentrating coarser pyroxenes in higher-energy settings and finer feldspars in lower-energy environments, while outer-shelf/slope deposits are largely biogenic and weakly river-influenced. Overall, compositional changes in correspondence with the key stratigraphic surfaces mark paleogeographic reorganizations and changes in sediment pathways. Because multiple drivers often act at once (e.g., tectonism, volcanism, and local autogenic effects), petrographic analysis should be integrated with facies, texture, and process data to isolate the forcing mechanisms better. These results demonstrate that sedimentary petrography can play an important role in the sequence-stratigraphic interpretation of a sedimentary succession, strengthening links between modern routing systems and the ancient record.

Keywords: sand composition; sequence stratigraphy; middle Pleistocene; Latium Tyrrhenian margin.

Submitted: 15 Agosto 2025 - Accepted: 16 September 2025

1. INTRODUCTION

Sedimentary petrography has traditionally been applied to provenance analysis to reconstruct the tectonic setting of source terranes (Dickinson, 1985) and to document compositional variations across stratigraphic successions in response to major paleogeographic reorganizations. Numerous studies have shown that sand composition can change across stratigraphic surfaces of different hierarchy and sequence-stratigraphic significance (Garzanti, 1991; Ito, 1991; Amorosi, 1995; Zuffa et al., 1995; Marchesini et al., 2000; Lawton et al., 2003; Basu et al., 2009; Garzanti et al., 2011; Villaseñor et al., 2020). However, its integration into sequence-stratigraphic analysis remains relatively underexplored (Zuffa et al., 1995; Amorosi and Zuffa, 2011). A combined petrographic and sequence-stratigraphic approach can enhance paleogeographic reconstructions and clarify the relative roles of tectonics,

eustasy, and climate in controlling sediment supply and dispersal pathways.

The composition of sandy sediments is regulated by both allogenic processes, such as tectonics, climate, and base-level fluctuations, and autogenic processes, such as sediment mixing, hydraulic sorting, and reworking. These processes operate over different temporal and spatial scales: long-term tectonics and climate oscillations can drive compositional changes within high-rank depositional sequences over millions of years (Zuffa et al., 1995; Garzanti et al., 2003), whereas short-term changes in sediment sources, routing, and depositional processes may dominate within low-rank sequences and across individual systems tracts (Amorosi and Zuffa, 2011). Not all sequences or systems tract boundaries are marked by sharp petrofacies changes, and compositional transitions may be gradual or absent altogether. Disentangling these effects requires high-resolution facies analysis, chronological control, and quantitative compositional data.

A source-to-sink perspective provides a powerful framework for understanding the processes that govern sediment production, transport, storage, and final deposition (Covault et al., 2013; Amorosi et al., 2016). Provenance studies based on petrographic modes can track sediment from source regions whose physiography, lithology, and tectonic history dictate the initial detrital signature through transfer zones and into depositional sinks. Along the sediment-routing system, this primary signal is progressively modified by chemical weathering, mechanical breakdown, mixing, and selective transport (Young et al., 1975; Nesbitt and Young, 1996; Garzanti et al., 2013; Garzanti, 2016). Nearshore and deep-marine environments further alter grain composition and texture through wave, tide, and current reworking, as well as diagenetic processes after burial (McBride, 1985; Garzanti et al., 2009, 2015 a,b). Understanding these transformations is essential to isolating the provenance signal from environmental overprints.

Quaternary continental-margin successions offer particularly valuable opportunities for such integrated studies. In these relatively young deposits, the stratigraphic architecture is often well constrained, source areas are known, and the timing of sea-level fluctuations is tied to orbitally driven glacial–interglacial cycles (Allen, 2017). This allows for more confident attribution of compositional changes to specific drainage reorganizations or shifts in sediment supply. Modern analogues can be analyzed to quantify the influence of individual processes, providing calibration for interpreting the ancient record and reducing the uncertainties introduced by post-depositional alteration.

In the Mediterranean region, modern sedimentary systems have been extensively characterized in terms of provenance, petrography, and depositional environments (e.g., Critelli and Le Pera, 1994, 2002; Garzanti et al., 2009, 2015 a,b). However, relatively few studies have linked modern compositional datasets directly to their preserved stratigraphic successions within a detailed sequence-stratigraphic framework (Garzanti et al., 2011; Tentori et al., 2016, 2018, 2021, 2022). The Quaternary succession of the Roman Basin provides an ideal case study for such an approach, as it has been framed into a detailed sequence-stratigraphic scheme (Milli, 1997, 1994; Milli et al., 2008, 2013, 2016). In fact, this basin preserves well-dated Pleistocene to Holocene fluvial, coastal, and deltaic, and shelfal deposits associated with the Tiber River and documents the role played by glacio-eustasy, tectonic uplift, volcanic activity, and autogenic processes in conditioning the sand composition of this Quaternary succession (e.g., Tentori et al., 2016, 2018).

This review paper synthesizes results from two complementary case studies (see Tentori et al., 2016, 2018), which include i) a high-resolution petrographic analysis of Late Lower Pleistocene to Holocene deposits of the high-rank composite Ponte Galeria Sequence (PGS), and ii) a compositional source-to-sink study of the modern Tiber River system that constitutes the product of the Holocene highstand sedimentation of the Tiber Depositional Sequence, which in turn represents the last of the low-rank sequences that form the PGS. By comparing the modern system with its Quaternary counterpart, we explore how compositional trends are recorded across different stratigraphic surfaces, evaluate the relative influence of allogenic and autogenic controls, and develop a conceptual model linking provenance, sediment composition, and stratigraphic architecture in a glacio-eustatically influenced continental-margin setting.

2. GEOLOGICAL SETTING

The Roman Basin develops along the central sector of the Latium Tyrrhenian margin. It stretches in the NW-SE direction for approximately 135 km north and south of the Tiber River (Fig. 1). It began to develop from the Late Pliocene due to the extensional tectonics connected to the opening of the back-arc Tyrrhenian Basin, in turn related to west-directed Apennine subduction (Malinverno and Ryan, 1986; Patacca et al., 1990; Doglioni et al., 2004). The basin is one of the NNW-SSE/NW-SE and subordinate NE-SW half-graben basins occurring along the Latium margin that were filled with syn-rift and post-rift clastic and volcaniclastic sediments (Funiciello et al., 1976; Cavinato et al., 1992; Mariani and Prato, 1988; Barberi et al., 1994) that were essentially transported and deposited by a Pliocene to Pleistocene fluvial system similar to the modern Tiber River and its tributaries (Fig. 2). The evolution of the Roman Basin has been accompanied by a continuous regional tectonic uplift (Milli, 1997; Bordoni and Valensise, 1998; Giordano et al., 2003) and intense volcanic activity, which reached its climax during the Middle-Upper Pleistocene with the development of the potassic-rich volcanic complexes of the Roman Magmatic Province (Sabatini and Albani complexes) (Conticelli and Peccerillo, 1992; Cioni et al., 1993; Karner et al., 2001; Peccerillo, 2005).

The consequence of this is that the stratigraphic setting

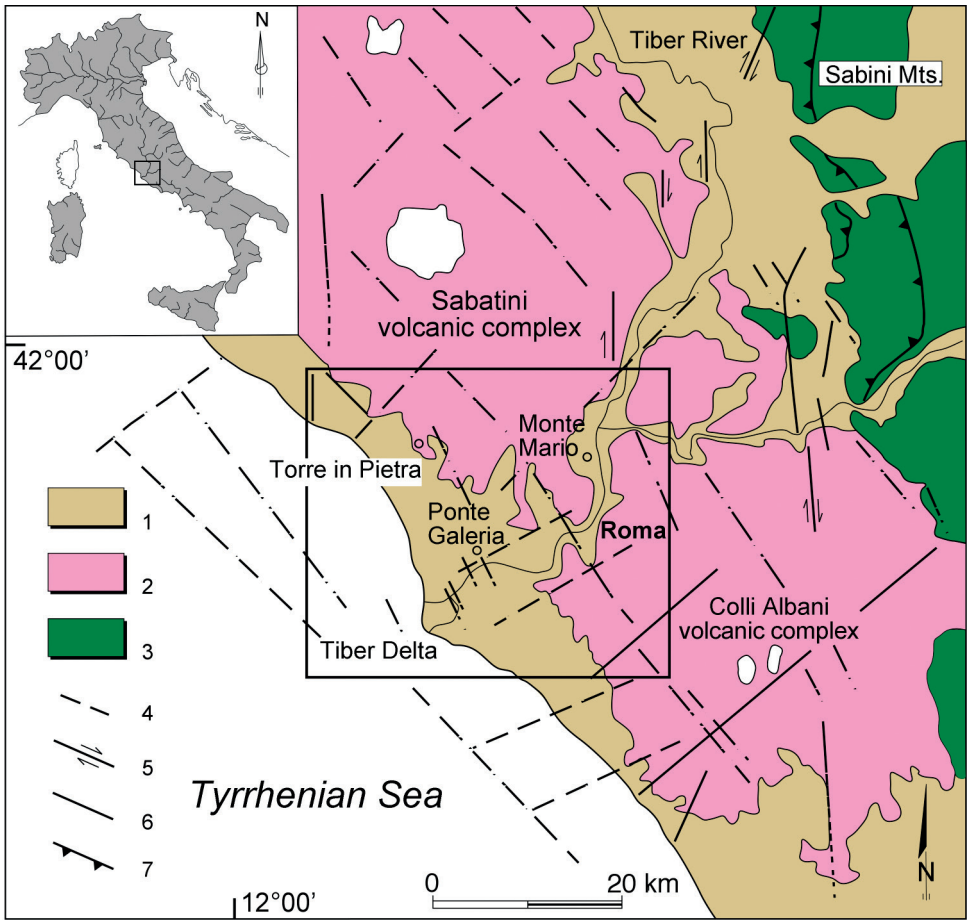

Fig. 1 - Simplified geological sketch of the central Tyrrhenian margin of Italy. (1) Messinian-Holocene sedimentary deposits; (2) Pliocene-Pleistocene lavas and volcaniclastic deposits; (3) Mesozoic–Cenozoic sedimentary deposits; (4) main buried faults; (5) strike-slip faults; (6) normal faults; (7) major thrusts. The black square indicates the fluvial downstream and marine study area (modified after Tentori et al., 2016).

of the Roman Basin reflects the close interaction between tectonic uplift, volcanic activity, and glacio-eustatic sea-level fluctuations related to Quaternary climatic changes (Cavinato et al., 1992; De Rita et al., 1994, 2002; Milli, 1994, 1997; Giordano et al., 2003; Mancini and Cavinato, 2005; Milli et al., 2008). The stratal architecture is, in fact, characterized by several depositional units constituting low-rank (high-frequency) depositional sequences (Mitchum and Van Wagoner, 1991; Posamentier and Allen, 1999; Catuneanu et al., 2011), with durations ranging from 30 to 120 kyr, stacked to form two composite high-rank sequences (low-frequency) named the Monte Mario Sequence (MMS; lower Pleistocene) and the Ponte Galeria Sequence (PGS; Late Lower Pleistocene to Holocene) respectively (Milli, 1997; Milli et al., 2013, 2016) (Fig. 3). The MMS deposits are known mainly through the stratigraphy of wells and limited outcrops and consist of coastal to transitional-shelf systems that developed during the late lowstand and transgressive systems tracts of the MMS. The absence of HST deposits is due to the erosion related to the sea-level fall that generated the sequence boundary of the PGS. The latter, in fact, constitutes a polygenic erosional surface formed during the sea-level fall between MIS 31 and MIS 20, along which the PGS deposits overlie the shelfal mud of the MMS.

The PGS crops out extensively between the city of Rome and the Tyrrhenian Sea, and contains fluvial, fluvio-lacustrine, barrier-lagoon, and transitional-shelf systems organized to constitute the lowstand (LST), transgressive (TST), and highstand (HST) systems tracts (Fig. 4). The occurrence in the PGS of pyroclastic and volcaniclastic deposits, deriving from the Albani and Sabatini volcanic complexes (Sottili et al., 2010; Marra et al., 2011, 2014), together with strontium isotopes data, was used to constrain the age and duration of the twelve low-rank sequences (from 5 to 80 m thick) that form the PGS.

The boundaries of the low-rank sequences are marked by sharp erosional surfaces recording basinward and downward facies shifts and by subaerial exposure and paleosol development in interfluvial areas. In particular, the low-rank sequences from PG01 to PG3 constitute the LST of the PGS; sequences from PG4 to PG8 are assigned to the TST, while the PG9 sequence, also known as the Tiber Depositional Sequence (TDS), developed entirely during the HST of the PGS (Milli et al., 2016) (Fig. 4). Note that the PGS shows an overall seaward stacking of low-rank sequences (Fig. 4), a trend opposite to that it would have been if controlled by glacio-eustatic alone.

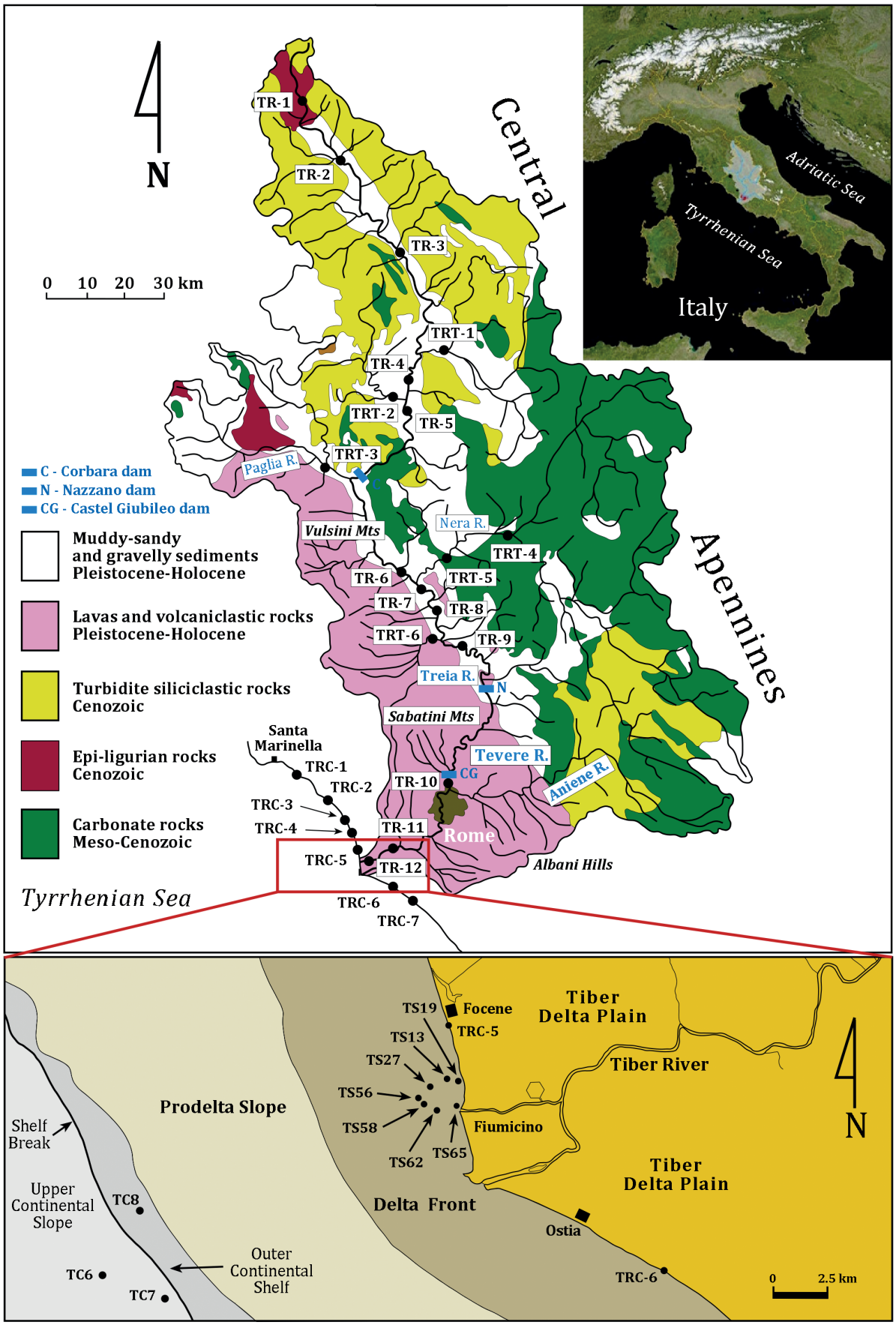

Fig. 2 - The map shows the track of the Tiber River and the main geologic units cropping out within its catchment. Sample locations that include the Tiber River (TR), its tributaries (TRT), foreshore (TRC), shoreface (TS), and continental shelf (TC), are indicated by numbered filled circles (modified from Tentori et al., 2016).

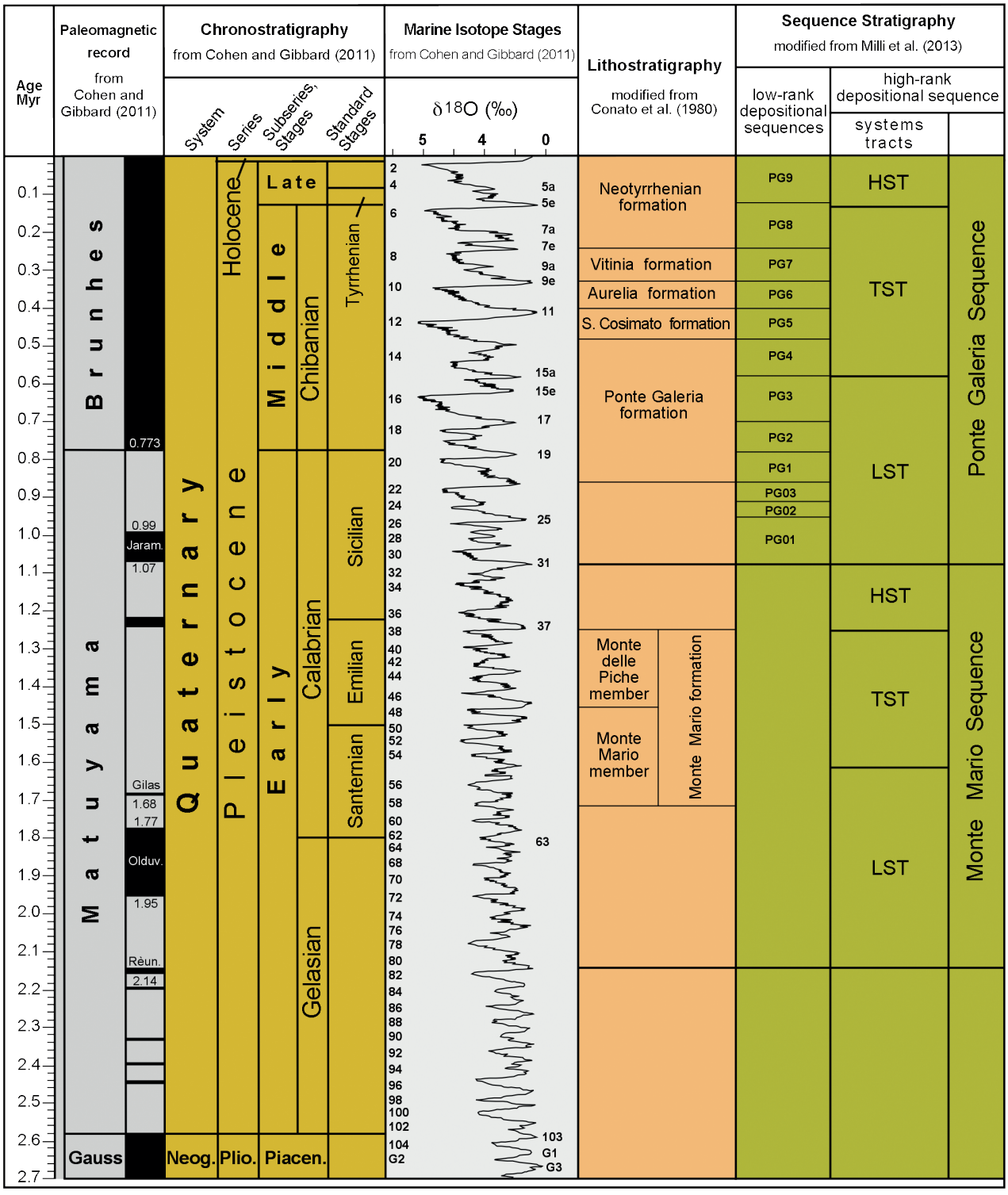

Fig. 3 - Chronostratigraphic and sequence-stratigraphic scheme of the Quaternary deposits of the Roman Basin (after Milli et al., 2013, 2016). HST: highstand systems tract; TST: transgressive systems tract; LST: lowstand systems tract.

This suggests that the present stacking pattern of PGS is an expression of the combined effects of eustatic sea-level changes and regional tectonic uplift; the latter would have forced the seaward migration of the low-rank sequence equilibrium points, thus helping to define the final stacking pattern of PGS (Milli, 1997; Milli et al., 2008).

Among the twelve low-rank sequences forming the PGS, the Tiber Depositional Sequence is the most complete and developed during the last glacial-interglacial cycle of post-Tyrrhenian age (last 120 kyr) (Milli et al., 2013, 2016) (Fig. 5). The lower boundary is an erosional surface formed during the sea-level fall following the

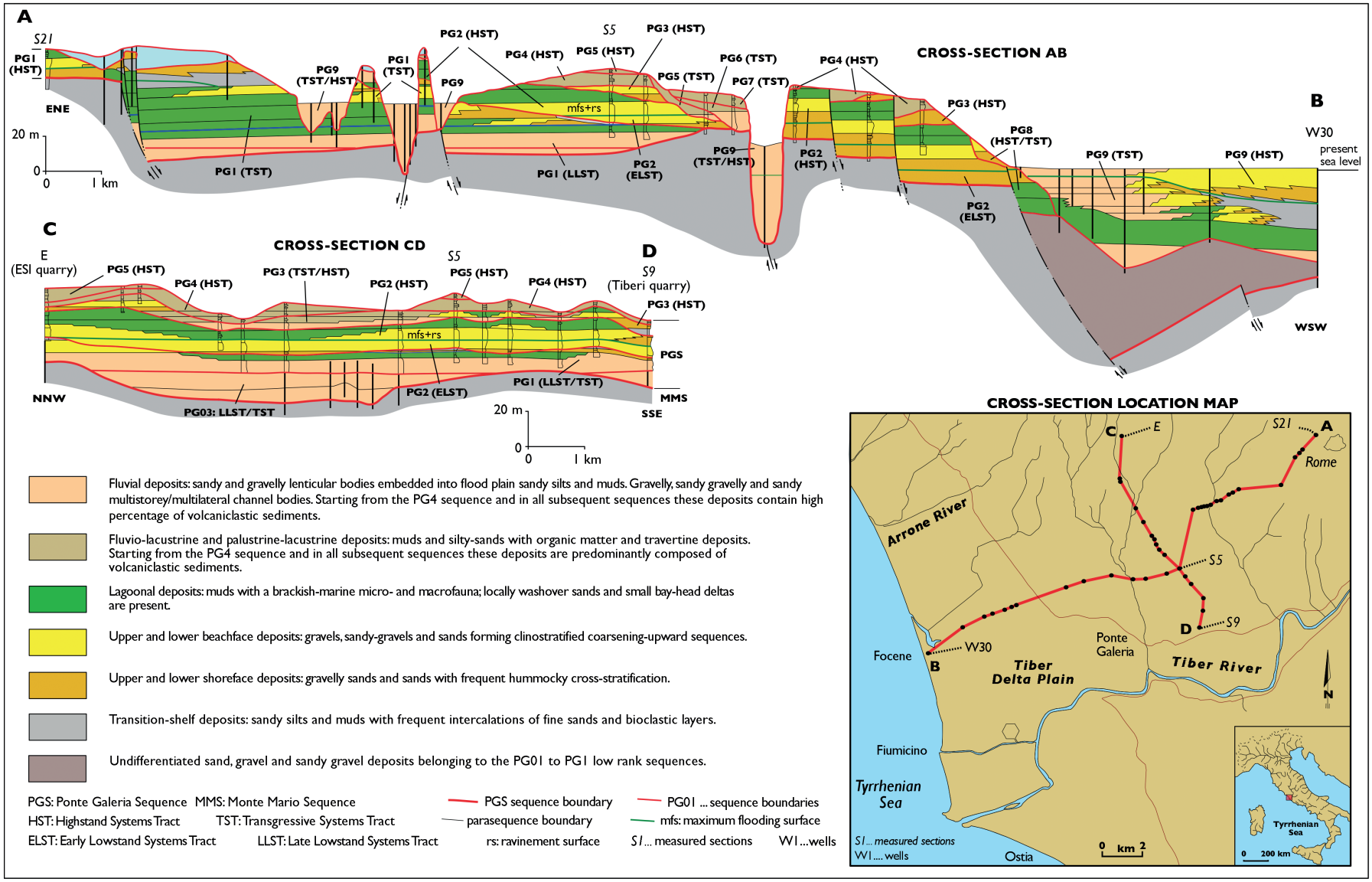

Fig. 4 - A-B, C-D) Stratigraphic cross-sections displaying the depositional architecture of the composite high-rank Ponte Galeria Sequence (modified after Milli, 1997). E) Conceptual sketch showing the stratigraphic relationships among low-rank sequences in the Roman Basin, driven by the interplay between tectonic uplift of the Latium-Tyrrhenian margin and eustatic sea-level change during development of the high-rank Ponte Galeria Sequence. Note the progressive downward and seaward migration of the low-rank sequences in response to uplift of the continental margin.

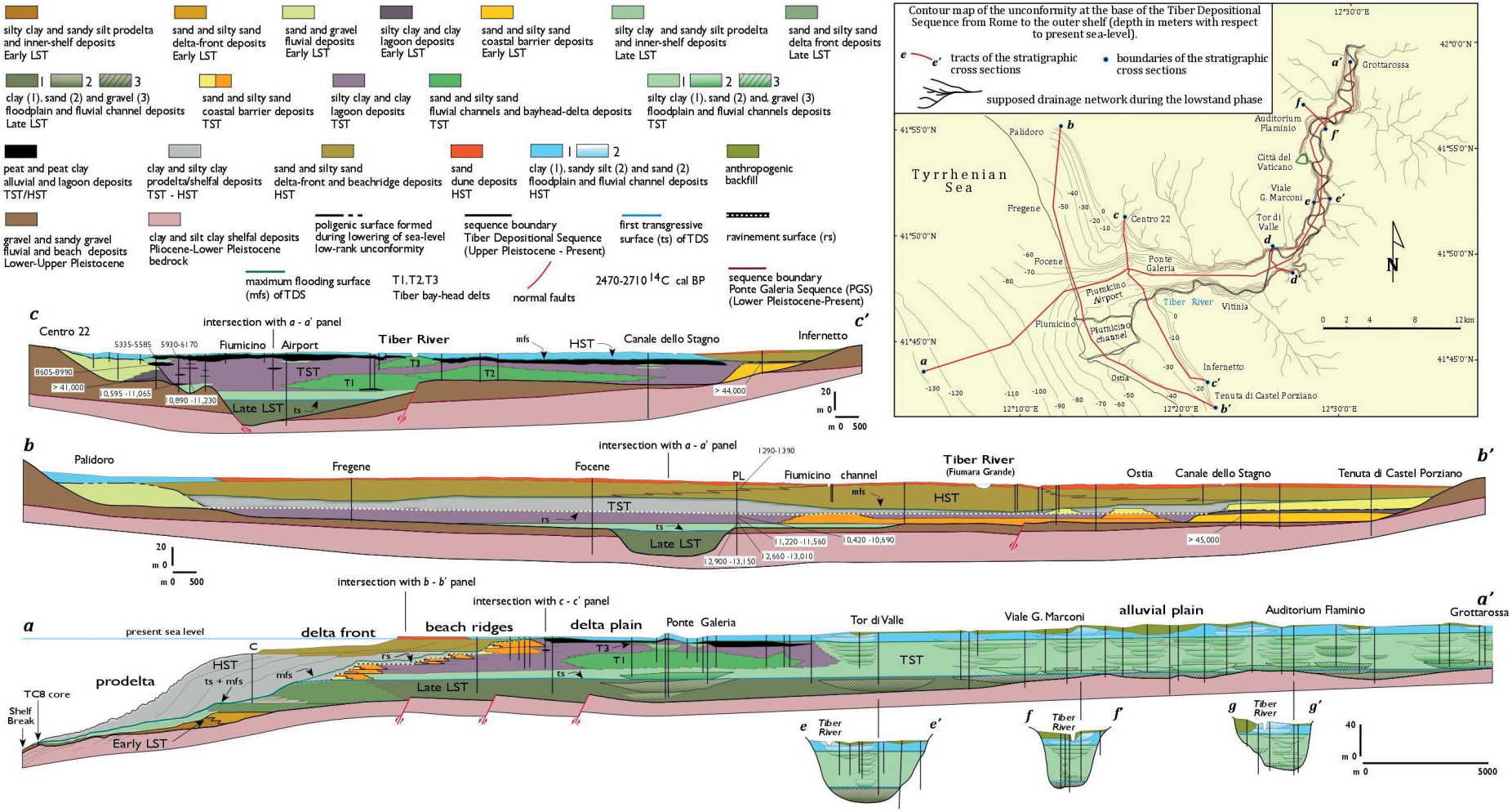

Fig. 5 - Stratigraphic cross-sections displaying the depositional architecture of the Tiber Depositional Sequence (from Milli et al., 2016).

MIS 5.5 highstand. The upper boundary corresponds to the modern depositional surface. The TDS succession, which ranges from less than 1 m to 80 m thick, records the transition from a wave-dominated estuary to a wave-dominated delta. Its internal architecture comprises a lowstand systems tract formed during valley incision and early infilling with fluvial, lagoonal, and beach deposits; a transgressive systems tract characterized by retrogradational stacking pattern of a sinuous fluvial system, a few bayhead deltas, a barrier–lagoon system, and a shelf depositional system, and a highstand systems tract represented by the progradation of the wave-dominate Tiber delta, downlapping onto the present outer shelf (Bellotti et al., 1994; Milli et al., 2016).

The ancient fluvial system that supplied the PGS during the Quaternary was probably equivalent to the present Tiber River system. The latter, which originates in the Apennine mountains, flows for 406 km, draining an area of 17,375 km^2. The catchment includes carbonate, siliciclastic, and volcanic rocks ranging in age from Mesozoic to Quaternary. The Apennine belt contains ophiolitic sequences and Meso-Cenozoic pelagic to platform carbonates, associated with synorogenic turbiditic sediments deposited during the Oligocene–Miocene in a foreland-basin system. The sandy turbidites are feldspatho-quartzose to litho-feldspatho-quartzose, with common metamorphic, plutonic, sedimentary, and volcanic lithic fragments (Gandolfi et al., 1983; Valloni and Zuffa, 1984; Gandolfi and Paganelli, 1993; Gandolfi et al., 2007; Amendola et al., 2016; Stalder et al., 2018). The Tiber catchment lies within the Latium-Campania Superprovince (Garzanti et al., 2002), and the composition of its sands reflects recycling of Miocene turbidites, exposure of Mesozoic carbonates, and Quaternary potassic and ultrapotassic volcanism of the Roman Magmatic Province. Modern Tiber sands and deltaic deposits contain quartz, feldspars, and minor terrigenous lithics from foredeep turbidites; limestone and chert from the Umbria pelagic succession; and subordinate volcanic detritus, including rare volcanic lithics and crystals of leucite and sanidine (Garzanti et al., 2002). These same components, in variable proportions, are observed in PGS deposits.

3. METHODS

This study integrates fieldwork and laboratory analyses to investigate compositional variability in both ancient and modern deposits of the Tiber River system within the framework of the Ponte Galeria Sequence (PGS). Fieldwork in the Roman Basin targeted low-rank depositional sequences of the PGS, with facies analysis and systematic sampling from newly measured and previously described sections into two quarries (Tiberi and ESI quarries), and at the Torre in Pietra outcrop (Milli, 1997; Milli and Moscatelli, 2001; Tentori et al., 2016) (Fig. 6). Twenty-nine sand samples were collected from the Tiberi quarry (TQ1-TQ15) (Fig. 7), ESI quarry (EQ1-EQ11) (Fig. 8), and Torre in Pietra (TO1-TO3), encompassing Early to Middle Pleistocene deposits from PG1 to PG7 (Fig. 9). Sampling was designed to capture petrographic variability across sequence boundaries and within facies associations corresponding to different systems tracts to evaluate the relative influence of autogenic processes (sedimentary processes, provenance mixing, hydraulic sorting) and allogenic controls (tectonism, eustasy, volcanism).

The TDS (PG9) was sampled in greater detail due to its stratigraphic completeness and relevance for highstand conditions. Eighteen stream-sand samples were collected from the modern Tiber River (TR1-TR12) and its major tributaries (TRT1-TRT6) at approximately 30 km intervals from the headwaters to the lower reaches, with tributaries sampled just upstream of their confluence with the main river (Fig. 2). Seven additional sand samples were collected from the swash zone of beaches north and south of the Tiber mouth (TRC1-TRC7) to assess the effects of littoral drift, wave, and current reworking and to compare the composition of modern coastal sands with the HST coastal deposits of older low-rank sequences with those of the TDS.

Offshore sampling of the TDS targeted the delta-front and prodelta settings. Twenty-one sand samples were collected from gravity cores on the delta front at various intervals (Fig. 10), allowing detailed stratigraphic and compositional analyses to track changes through time (Milli et al., 2016). An additional twenty-one samples were collected from three gravity cores (TC6, TC7, TC8) retrieved from the submerged delta sector off the river mouth. Core TC6 was recovered from an incised gully on the continental slope at 240 m water depth, while TC7 and TC8 were drilled on the continental shelf near the shelf break at 155 m and 126 m water depth, respectively (Di Bella et al., 2013) (Fig. 11). Data from these cores were compared with published results from the Ocean Drilling Program (ODP) Site 974, Leg 161 (Marsaglia et al., 1999), previously interpreted as containing Tiber-derived sediment.

In total, 67 thin sections from PGS and modern samples and 52 thin sections from the TDS offshore cores were prepared and stained for potassium and calcium feldspar following the method of Marsaglia and Tazaki (1992). Petrographic point-counting was performed with the Gazzi-Dickinson method (Ingersoll et al., 1984), counting 400 points per slide. Lithic, monomineralic, and biogenic grains were classified according to Zuffa (1980, 1985, 1987, 1991), Marsaglia (1992), and Marsaglia et al. (1999). For TDS offshore samples, grains were grouped as noncarbonate extrabasinal (NCE), carbonate extrabasinal (CE), and carbonate intrabasinal (CI) after Zuffa (1980).

Medium-sand fractions were selected for compositional analysis to maintain consistency with previous provenance studies (e.g., McBride and Picard, 1987). To evaluate potential grain-size dependence, selected samples were also analyzed in fine and very fine sand fractions, including TQ4, TQ7, TQ12, TQ15, EQ2, EQ5, TR11, and 15 fine-

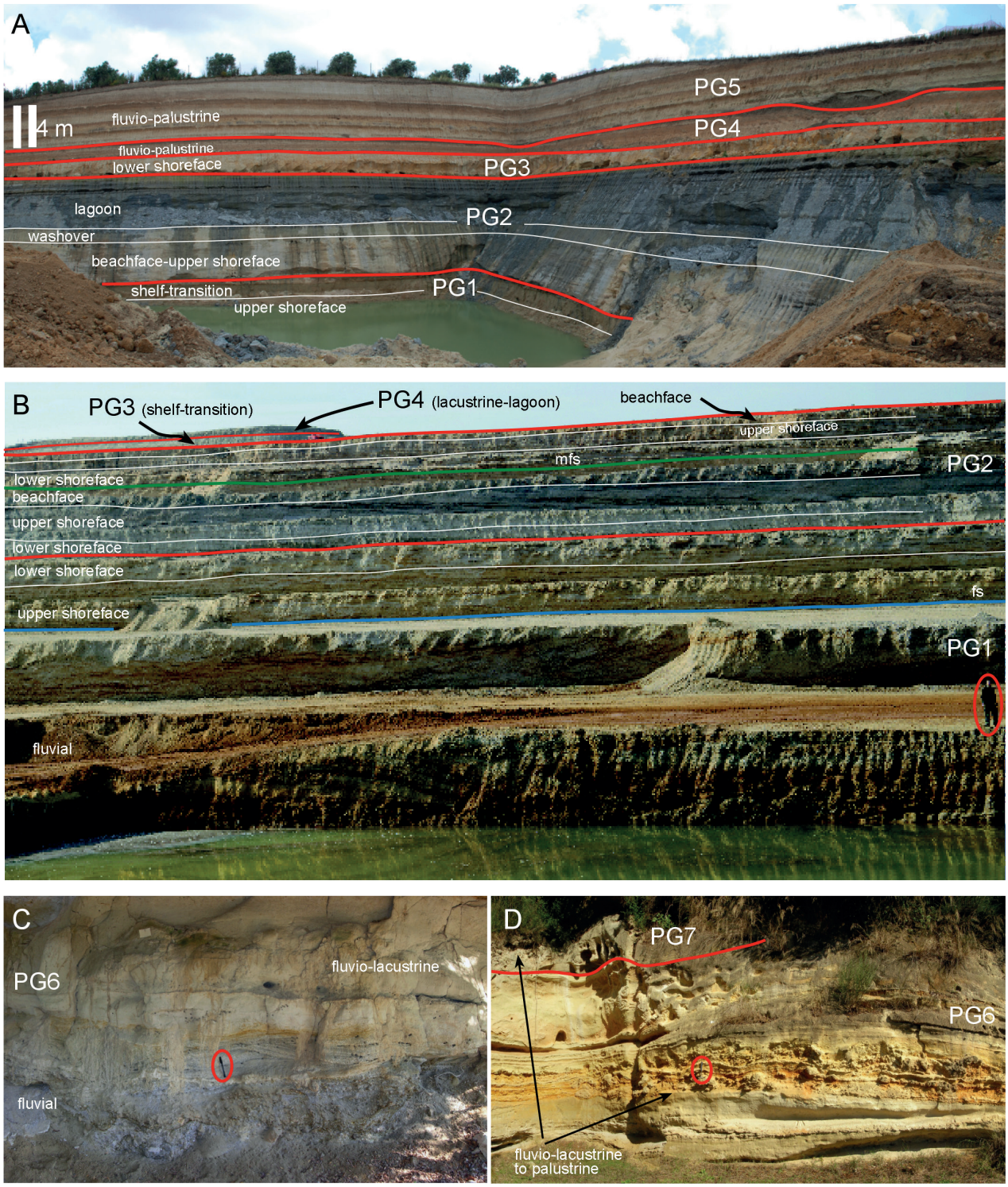

Fig. 6 - Field photographs showing the environmental and sequence-stratigraphic interpretations of the deposits cropping out in the ESI quarry (A), the Tiberi quarry (B), and the Torre in Pietra locality (C-D). Scale indicators: man (B), pencil (C), and hammer (D) (slightly modified from Tentori et al., 2016).

grained TDS samples from delta-front and prodelta settings. Modal compositions were plotted on QFL ternary diagrams following Garzanti (2016), with nomenclature from Crook (1960), Dickinson (1970), and Weltje (2006), and on lithic proportion diagrams for provenance interpretation (Zuffa, 1980, 1987, 1991; McBride and Picard, 1987; Veermesch et al., 2016).

Grain roundness was measured to assess resistance to transport and mechanical abrasion in both fluvial and coastal settings. Mean roundness values were determined for medium-sand monocrystalline quartz and carbonate lithic fragments [Lsc(cry)+Lsc(mic)], following McBride

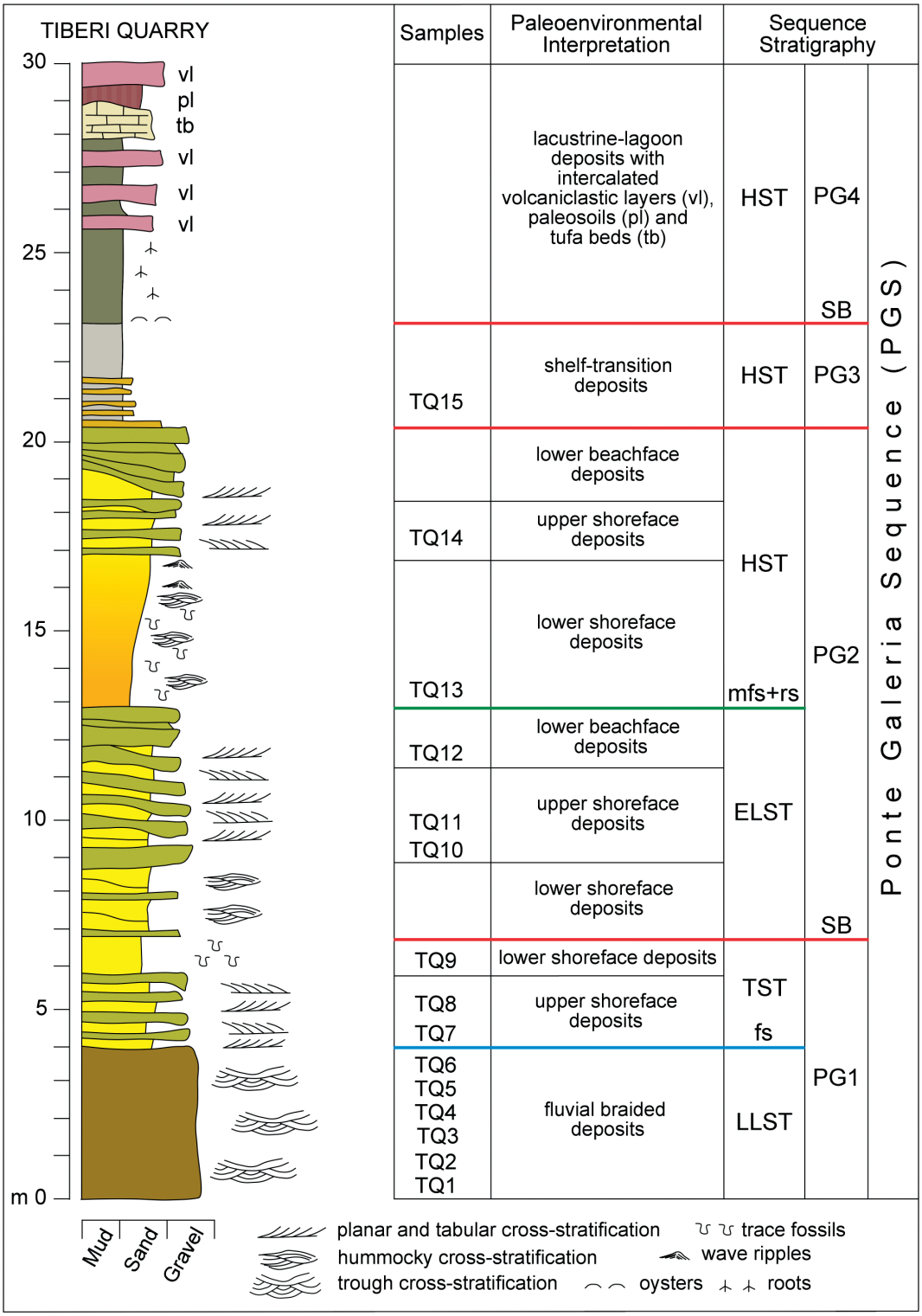

Fig. 7 - Stratigraphic log of Tiberi quarry showing the sampled intervals (TQ), the inferred depositional environment, and the sequence-stratigraphic interpretation (modified after Tentori et al., 2016).

and Picard (1987). The first 30 grains encountered during point counting were assigned numerical values from 1 (very angular) to 6 (well-rounded), and mean roundness values were calculated for each sample for comparison across the modern river, coastal transects, and Pleistocene deposits of the Tiber succession.

The combined datasets from ancient and modern environments were used to construct models of compositional trends from source to sink, enabling direct comparison between modern sediment-routing dynamics and their preserved Quaternary counterparts in the PGS and TDS.

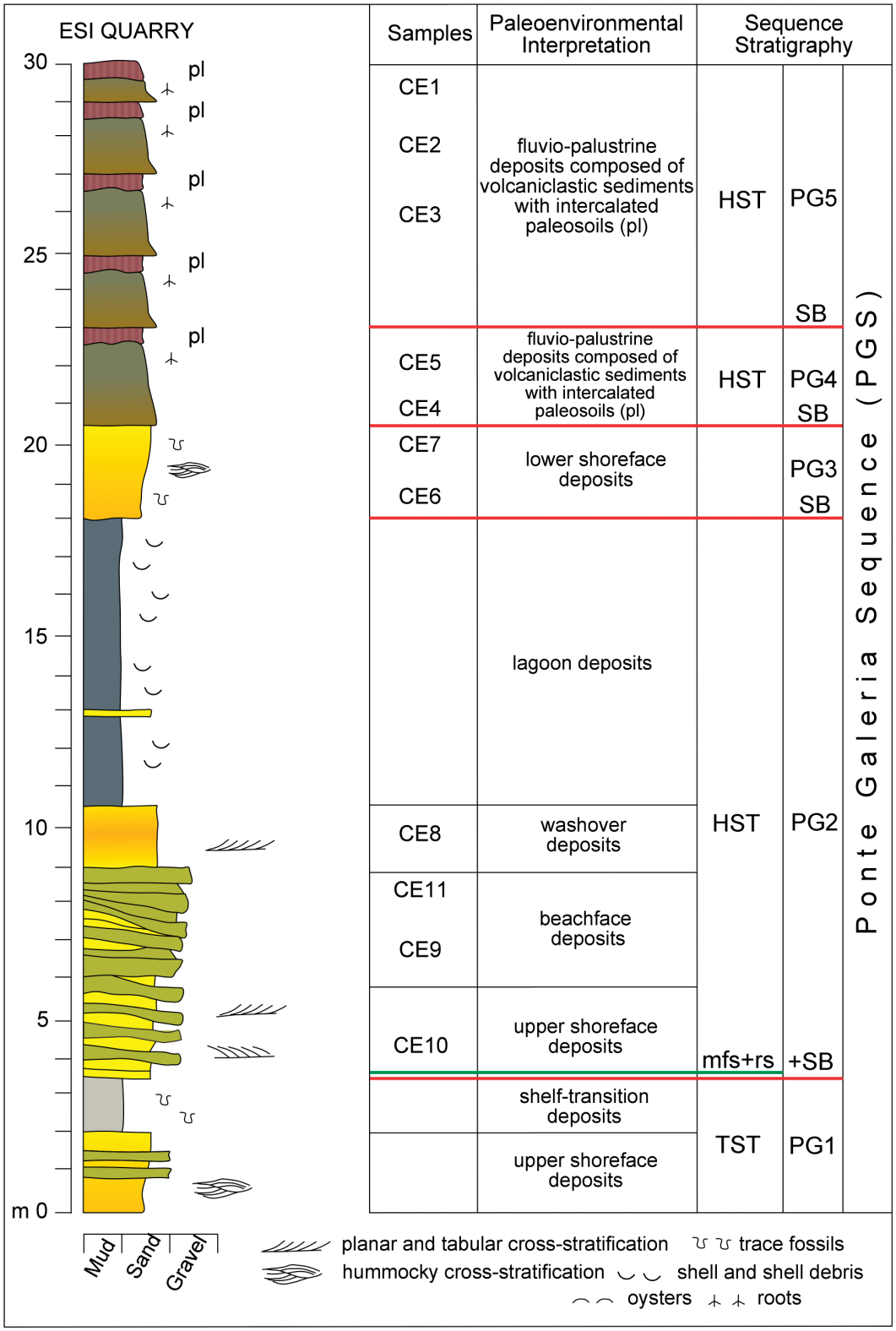

Fig. 8 - Stratigraphic log of ESI quarry showing the sampled intervals (EQ), the inferred depositional environment, and the sequence-stratigraphic interpretation (modified after Tentori et al., 2016).

4. RESULTS

The sand samples from the Ponte Galeria Sequence (PGS) exhibit wide variability in quartz, lithic, and feldspar proportions, with quartz and/or lithics generally dominating over feldspar except in a few cases (Fig. 12). Modal compositions range from feldspatho-quartzo-lithic to feldspatho-lithic-quartzose, with subordinate feldspatho-quartzose, litho-quartzose, quartzo-lithic, litho-feldspathic, feldspathic, and lithic types. Ancient

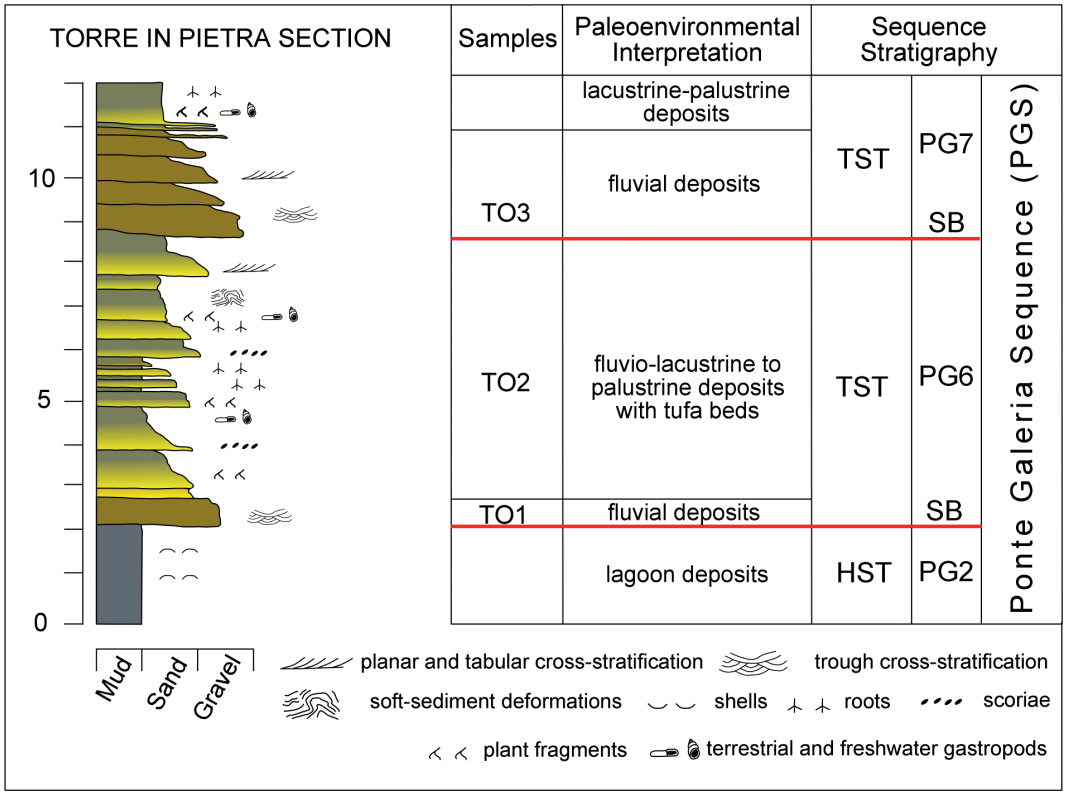

Fig. 9 - Stratigraphic column of Torre in Pietra outcrop showing the sampled intervals (TO), the inferred depositional environment, and the sequence-stratigraphic interpretation (modified after Tentori et al., 2016).

and modern samples were plotted separately by systems tract on QFL, Lm-Lv-Ls, and NCE-CE-CI ternary diagrams (Zuffa, 1980) to examine relationships between composition and sequence stratigraphic position (Figs. 13, 14). On these plots, the lowstand (LST), transgressive (TST), and highstand (HST) systems tracts are not cleanly separated, showing significant compositional overlap, particularly for the LST coastal-marine facies from the Tiberi Quarry.

Better discrimination was achieved using the parameter-ratio approach of Ito (1994), originally applied to forearc facies in the Boso Peninsula, Japan. In figure 15, TST samples form a distinct cluster, whereas HST samples show a transitional spread from the TST cluster and minor overlap with LST samples at low Lv/Lt values. This allowed the definition of three petrofacies: Petrofacies A (LST), Petrofacies B (TST), and Petrofacies C (HST).

Petrofacies A is characterized by abundant quartz, significant feldspar, and generally minor carbonate and metamorphic lithic fragments, with few samples rich in volcanic lithic grains (mean=NCE91CE8CI1). Petrofacies B contains abundant feldspar, significant volcanic lithic fragments, and minor quartz. The volcanic lithics show highly altered glassy groundmass, and PG5 samples are dominated by disaggregated soil aggregates, feldspar (>50%), and pyroxene. This petrofacies has a strong noncarbonate extrabasinal signature (mean= NCE98CE2CI0). Petrofacies C is rich in volcanic-lithic and siliciclastic sedimentary fragments and contains significant extrabasinal carbonate grains (mean= NCE74CE26CI0); pyroxenes are notably abundant in the coastal deposits.

Modern Tiber River and tributary sands (TR1-TR12; TRT1-TRT6) and foreshore samples (TRC1-TRC7) are described in detail in Tentori et al. (2016). Offshore samples from the delta front and prodelta provide additional insights into the composition of recent highstand deposits (Tentori et al., 2018).

In the upper and lower shoreface deposits of the delta front, the dominant components are monomineralic quartz and feldspar grains, along with sedimentary lithic fragments. Pyroxene and micas (biotite, muscovite, chlorite) are common accessory minerals. Minor constituents include opaque and non-opaque dense minerals, serpentine grains, and alterites-opaque to semi-opaque finely crystalline masses produced during weathering, lacking internal structures and potentially derived from altered monominerals or lithic fragments (Johnsson, 1990). Polycrystalline grains include quartz and chert, and carbonate bioclasts, both intrabasinal (mainly foraminifera) and extrabasinal, are common, being particularly abundant in cores 56 and 58. Siliciclastic sedimentary lithics consist of feldspathic and lithic siltstone, with minor mudstone; carbonate lithics include sparitic and micritic limestones. Volcaniclastic lithics display felsitic, vitric, and lathwork textures, with pumice and colorless, black, brown, and altered glass, and tuff fragments; phenocrysts include feldspar and pyroxene.

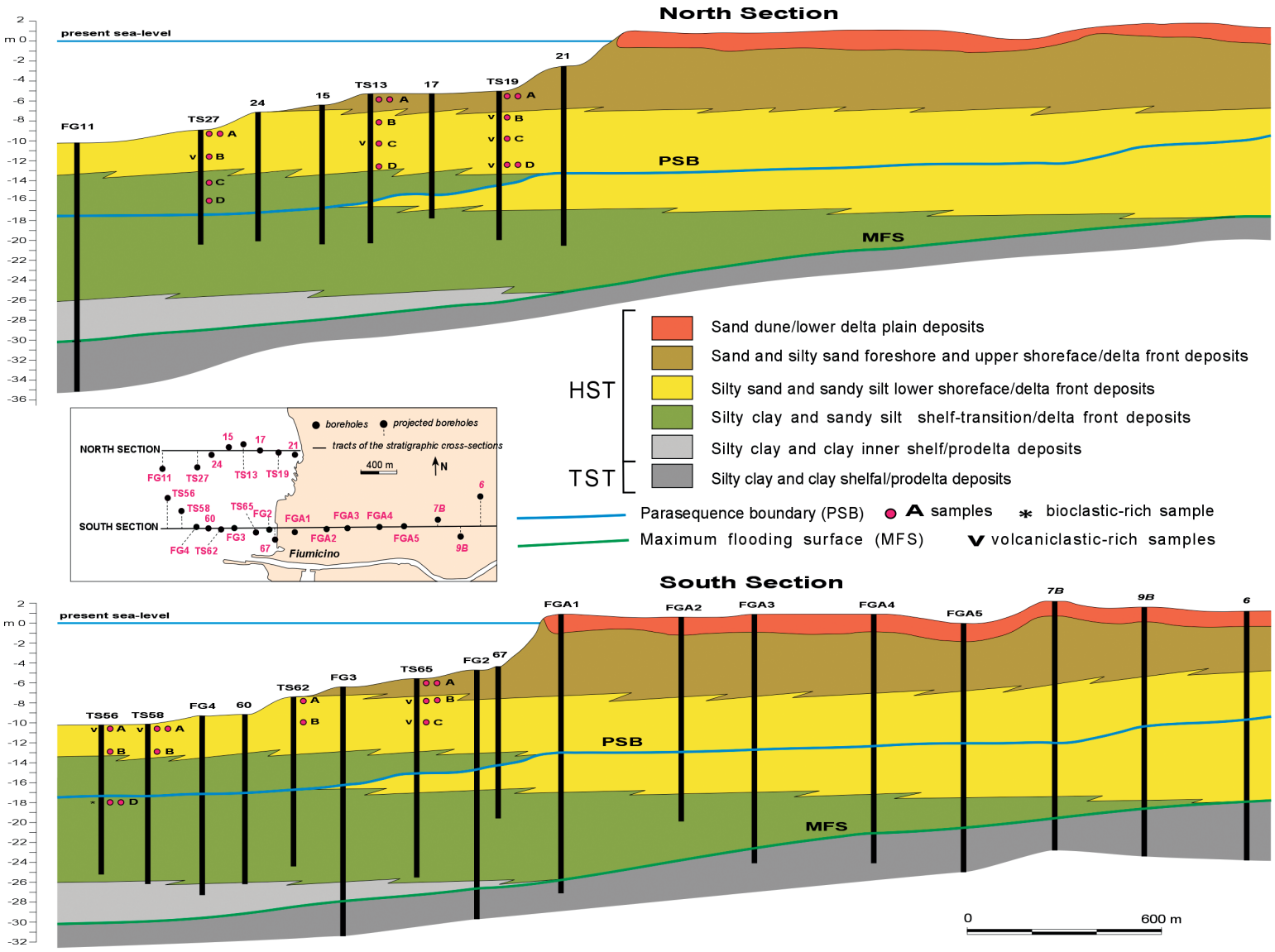

Fig. 10 - Stratigraphic sections and shoreface core locations in the northern (A) and the southern sectors (B) off the Tiber River mouth. Red dots indicate medium-grained sands and black dots fine-grained sands from cores TS13, TS19, TS27, TS56, TS58, TS62, TS65, and intervals A-D. All volcanic-rich samples occur within the yellow lower shoreface facies, while the bioclastic-rich sample lies below the parasequence boundary (modified after Tentori et al., 2018).

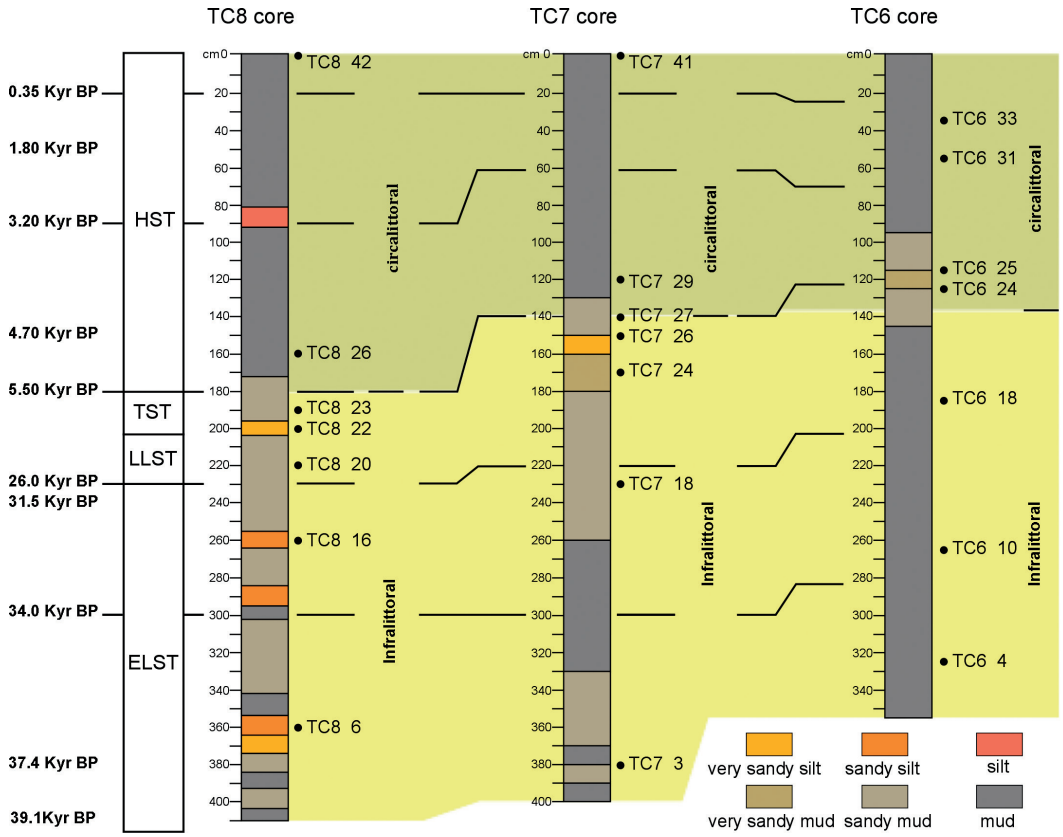

Fig. 11 - Lithology, sequence-stratigraphic interpretation, and location of the samples in the TC6, TC7, and TC8 continental shelf cores. Core locations are shown in figure 2. Modified from Di Bella et al. (2013).

Pyroxene grains are especially common (~20%) in medium-grained samples close to the river mouth (cores TS62, TS58, TS27) and inshore locations (TS19) but drop below 5% in finer sands. Micas are more abundant (~10%) in distal, fine-grained samples (TS58A, TS58B, TS56A, TS56D) compared to <5% in proximal medium sands. Volcanic lithic fragments are abundant in both medium-grained samples (TS65B, TS65C, TS58A, TS19C, TS13C) and fine-grained samples (TS56A, TS56D, TS27D).

On the continental shelf and slope, samples from gravity cores TC6, TC7, and TC8 (Fig. 11) are dominated by intrabasinal carbonate bioclasts (50-100%) (see also Di Bella et al., 2013). Exceptions occur in some TC6 intervals, which contain 20-40% monomineralic quartz and feldspar, with minor micas, pyroxene, amphibole, and dense minerals. Bioclasts include mollusks, echinoderms, red algae, bryozoa, and foraminifera, often diagenetically altered to siderite or unidentified minerals. Polycrystalline quartz and chert grains are present, while lithic fragments are relatively rare and include sparitic and micritic carbonate, siliciclastic, altered volcanic, and low- to medium-grade metamorphic types.

The combined dataset demonstrates that both ancient PGS sands and modern deltaic deposits preserve clear petrofacies trends linked to systems tracts while also recording significant spatial variability related to depositional setting, grain size, and sedimentary reworking.

5. DISCUSSION

The integrated petrographic dataset from the Ponte Galeria Sequence (PGS) and the modern Tiber system resolves three recurrent petrofacies that align with sequence-stratigraphic position and with shifts in forcing mechanisms through Quaternary time. In the high-rank PGS, Petrofacies A typifies lowstand (LST) fluvial and coastal sands and reflects erosion of siliciclastic turbidites in the upper drainage and carbonate successions in the middle to lower basin, with minor volcanic lithic input linked to the earliest, sporadic Sabatini eruptions. The close compositional and textural match between coeval beachface and fluvial sand indicates strong direct river control on the shoreface during lowstands, whereas along the modern coast, compositional maturity increases down-drift under sustained coastal reworking from the Middle Pleistocene to the Present. Petrofacies B, which characterizes transgressive (TST) fluvial and fluvio-lacustrine deposits where marine outcrops are absent, captures the rapid and voluminous arrival of volcaniclastic detritus from Sabatini explosive activity. The preponderance of altered vitric fragments and liberated K-feldspar and pyroxene records pedogenic overprint and chemical weathering in volcanics-rich units (Nesbitt and Young, 1996), consistent with soil formation on ash- and tuff-mantled surfaces. Petrofacies

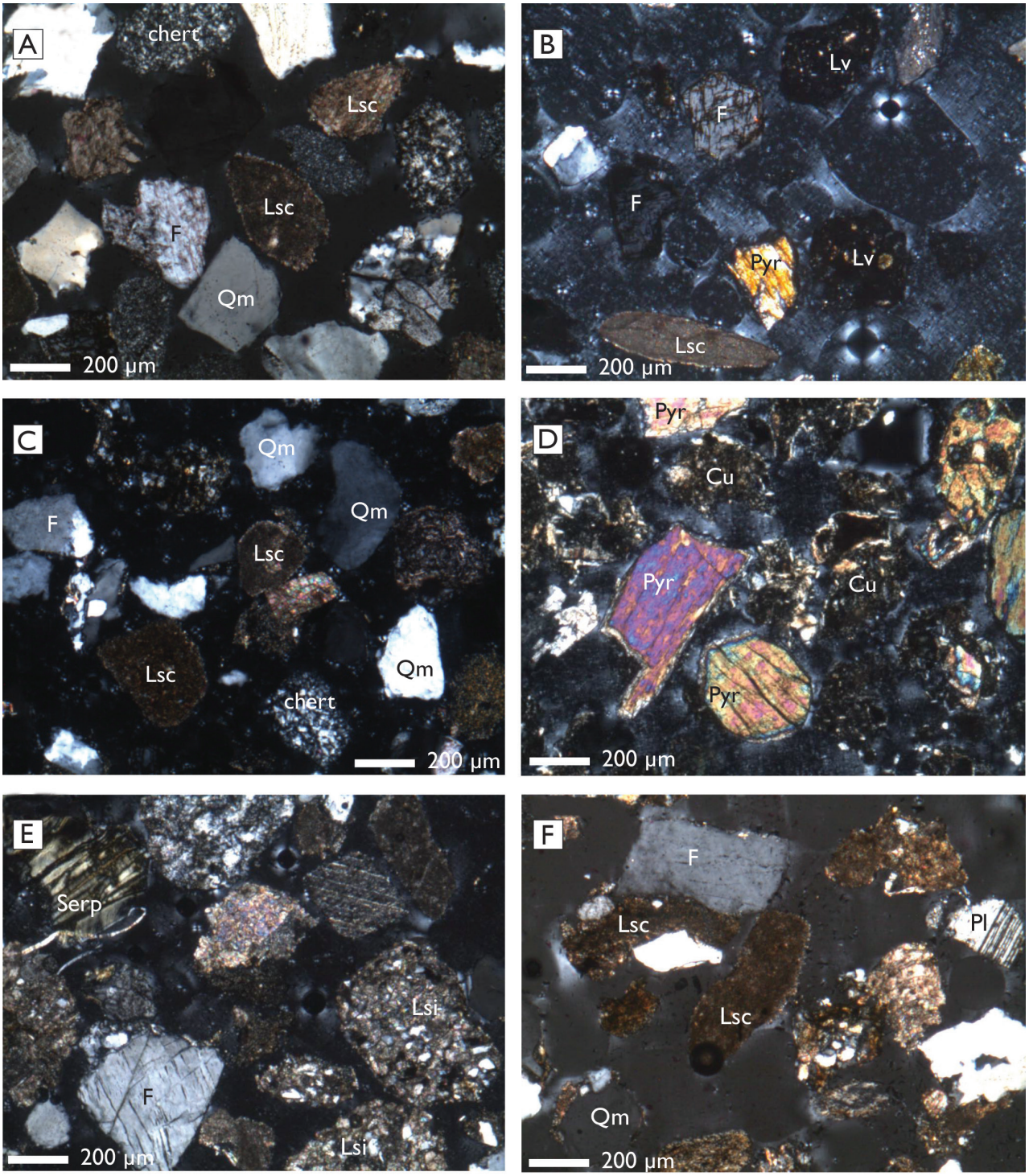

Fig. 12 - Photomicrographs from the Tiberi quarry (A-B), the ESI quarry (C-D), and modern Tiber River sands (E-F), highlighting key grain types. A) Lower-shoreface sample TQ9 with feldspar (F), monocrystalline quartz (Qm), and micritic carbonate lithic fragments (Lsc). B) Upper-shoreface sample TQ10 with feldspar (F), pyroxene (Pyr), volcanic lithic fragments (Lv), and micritic carbonate (Lsc). C) Beachface sample EQ1 with scarce carbonate lithic fragments (Lsc), quartz (Qm), and feldspar (F). D) Fluvio-palustrine sample EQ10 with pyroxene (Pyr) and cutan fragments (Cu) produced by soil alteration. E) Sample TR3 with serpentine (Serp), feldspar (F), and siltstone lithic fragments (Lsi). F) Sample TR5 with quartz (Qm), feldspar (F+Pl), and micritic carbonate lithic fragments (Lsc) (from Tentori et al., 2016).

C belongs to highstand (HST) fluvial and coastal deposits and reflects progressive reworking of volcanics-rich strata; preferential abrasion and dissolution of glass in lithic clasts release phenocrysts, especially pyroxene, while coastal processes winnow extrabasinal carbonate fragments relative to their riverine supply.

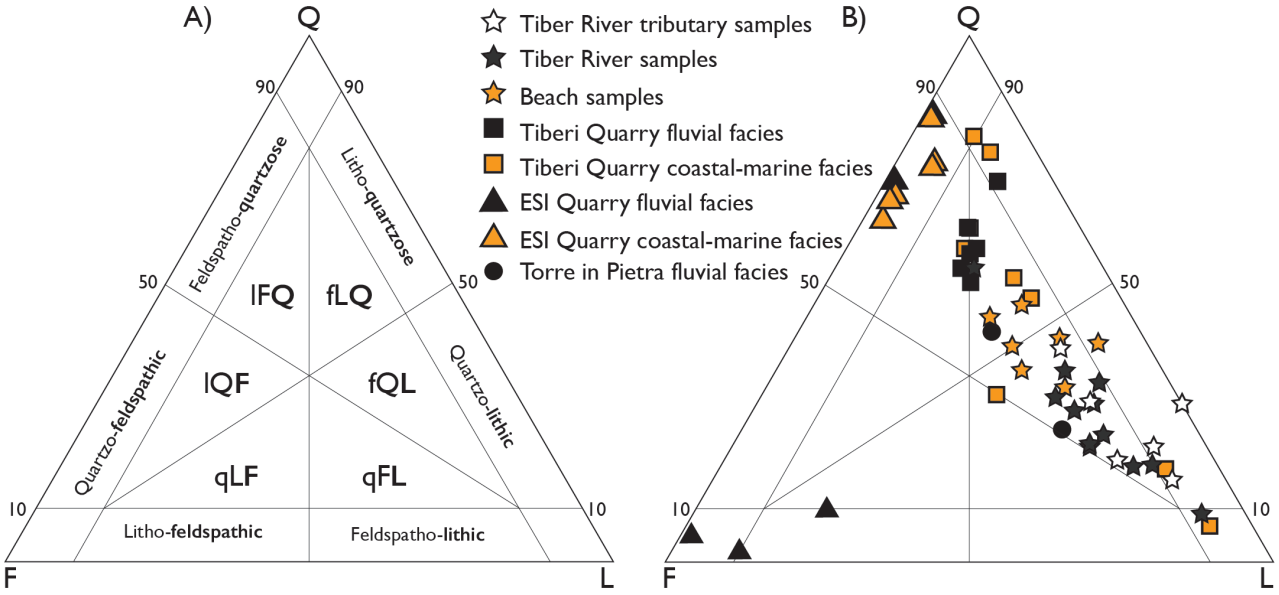

Fig. 13 - Ternary plots (A, B) used for the petrographic classification of the studied sand samples. Scheme A follows Garzanti (2016), which is based on the nomenclature of Crook (1960) and Dickinson (1970), and later adopted by Ingersoll (1983) and Weltje (2006). Q = quartzose; F = feldspathic; L = lithic; lFQ = litho-feldspatho-quartzose; fLQ = feldspatho-litho-quartzose; lQF = litho-quartzose-feldspathic; fQL = feldspatho-quartzo-lithic; qLF = quartzo-lithic-feldspathic; qFL = quartzo-feldspatho-lithic (from Tentori et al., 2016).

These petrofacies document how tectonic uplift, volcanism, and glacio-eustatic sea-level oscillations imprint differently on stratigraphic architecture and on sand composition. Regional uplift modulated source-rock exposure and the proportion of terrigenous detritus delivered across all systems tracts, whereas volcanism peaked during transgression, counteracting the typical TST reduction in clastic supply by injecting abundant juvenile debris via fall and pyroclastic density currents, with subordinate input from lava erosion. Eustasy governed base-level and river energy (Milli, 1997; Milli et al., 2008), strongly influencing sediment supply and coastal redistribution, especially where highstand shore-parallel currents enhanced lateral sorting. During lowstands, minimized accommodation and bypass favored a close source-sink linkage, explaining wide compositional scatter that likely tracks subcatchment-scale variations in rainfall and discharge, as in modern analogs (e.g., Leombruni et al., 2009). With the ensuing transgression, volcaniclastic influx reached a maximum, diluting carbonate sedimentary lithics; syndepositional and post-depositional alteration of vitric components further modified these signatures (Castorina et al., 2015). Reworking in marginal-marine settings during highstand progressively reduced volcanic lithic proportions, with beach sands showing increased quartz and decreased extrabasinal carbonates relative to fluvial counterparts as waves and wind intensified textural and compositional maturity.

Translating these trends to the constituent low-rank sequences clarifies time-scale dependencies and preservational biases. Pre-volcanic PG01-PG3 contain sparse tephra and are dominated by monomineralic quartz over lithic fragments; at the LLST-TST transitions, reduced fluvial flux during relative sea-level rise, combined with eolian and wave abrasion and longshore/rip-current reworking, preferentially removed softer extrabasinal carbonate grains while quartz survived, with HST conditions broadly restoring LLST-like NCE/CE and Q/L proportions. Upsection, increasing volcanic lithics and phenocrysts register the progressive volcaniclastic contribution to the paleo-Tiber. Syn-volcanic PG4-PG8 reflect a dual provenance-direct juvenile input from explosive eruptions plus cannibalization of older pre-volcanic units, accentuated by uplift and sea-level change-yielding low sedimentary and high volcanic lithic contents and promoting seaward stacking. Post-volcanic PG9, represented by modern fluvial-to-coastal sediments, captures the present connectivity between the inner/middle catchment and the river mouth (Figs. 16 and 17). Upstream sands integrate Jurassic ophiolites, Jurassic-Oligocene carbonates and siliciclastics, and Miocene foredeep turbidites, supplying quartz, K-feldspar, plagioclase, dense minerals, and siliciclastic and metasedimentary lithics, with serpentine textures indicating both direct ophiolitic erosion and recycling through Oligo-Miocene turbidites (see also Garzanti et al., 2002; Amendola et al., 2016). Middle-basin sands retain similar Q/F and dense-mineral proportions but lose serpentine, consistent with recycling of Miocene turbidites and Umbria-Marche carbonates. Downstream, K-feldspar rises relative to plagioclase, reflecting the high-K Roman Magmatic Province signature; carbonate lithics decline by dilution and abrasion during transport (McBride and Picard, 1987), with the highest grain-roundness values reached near the coast. In Rome and the lower basin, volcaniclastic deposits and subordinate lavas

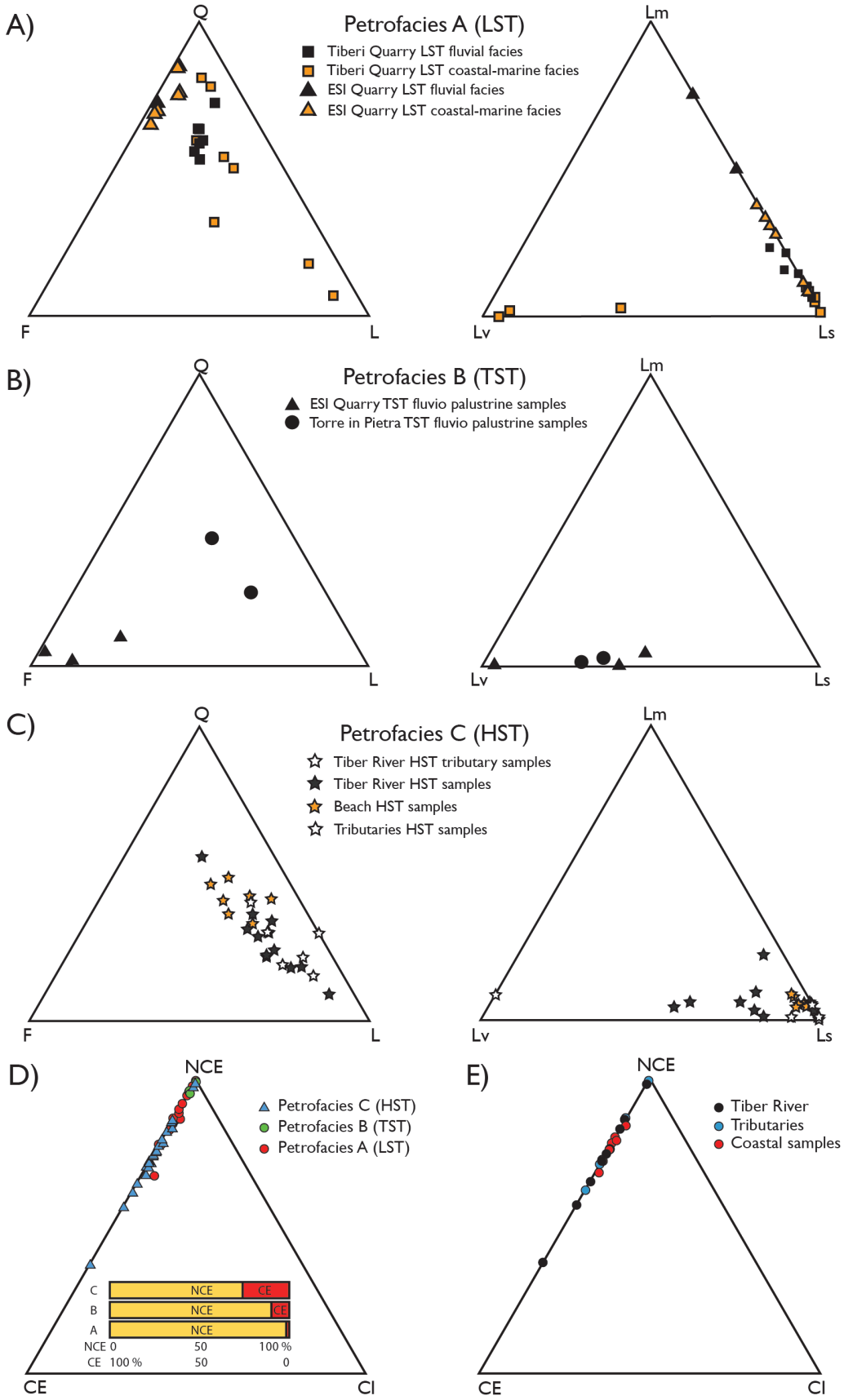

Fig. 14 - A-C) Quartz (Q), feldspar (F), and lithic (L) ternary plots, with lithic types subdivided into metamorphic (Lm), volcanic (Lv), and sedimentary (Ls), for the PGS petrofacies associated with HST, TST, and LST deposits. D) NCE-CE-CI ternary plot for the PGS petrofacies, accompanied by histograms showing relative percentages of NCE and CE (CI values are minimal, <1%, and excluded from the histograms). E) NCE-CE-CI ternary plot for PGS highstand systems-tract samples by depositional environment (from Tentori et al., 2016).

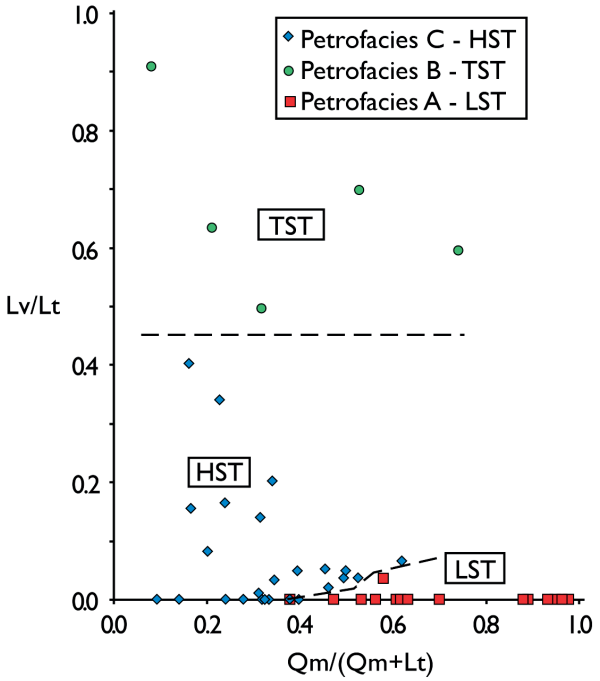

Fig. 15 - Compositional variation of PGS petrofacies, expressed through parameters and ratios following Ito (1994) (from Tentori et al., 2016).

contribute feldspar and pyroxene both as detrital grains and as phenocrysts within lithics, though these lithics are highly labile to dilution and abrasion (Cameron and Blatt, 1971; Critelli et al., 1997). Along the Lazio shoreline, beach sands reflect a mixture of Tiber input, deltaic reworking, and local supply; quartz increases relative to the river, pyroxene becomes prominent north of the mouth where small volcanic-draining rivers feed the coast, vitric fragments weather to release phenocrysts, and siliciclastic lithics likely derive from coastal outcrops of metamorphic-lithics-bearing turbidites and are transported south by longshore drift (Bellotti et al., 1993).

Process overprints that modify primary provenance signals are pervasive and quantifiable. Chemical weathering and pedogenesis reduce carbonate and volcaniclastic lithic percentages in both outcrop and soils (McBride, 1985), as shown by recalculated QFL excluding carbonate lithics (QFL-c), which isolates volcanic contributions without the confounding dissolution effect. During Sabatini paroxysm (PG4-PG8), glassy debris is intensely altered in paleosols, leaving K-feldspar and pyroxene enrichment and largely altered plagioclase within clay-rich horizons, with bulk geochemistry diverging from reworked tephra (Nesbitt and Young, 1996; Borrelli et al., 2012; Castorina et al., 2015). In the post-volcanic coast, phenocrysts are concentrated relative to volcanic lithics, consistent with coastal reworking that both liberates dense phases and preferentially destroys labile vitric fragments. Hydraulic sorting imposes predictable grain-size-composition relationships: across ancient quarries and modern river samples, finer fractions carry less quartz and more feldspar and lithics; fine sand enriches in K-feldspar relative to plagioclase, and lithic trends vary by local mixing and episodic tephra input (see, for example, Garzanti et al., 2009; James et al., 2007; Marsaglia et al., 2010; Garçon et al., 2014; Garzanti et al., 2015 a,b). Mechanical abrasion further removes labile clasts and increases roundness down-system: quartz and carbonate grains evolve from subangular upstream to subrounded downstream; carbonate lithics-and micrite more than sparite-round faster than quartz, and beach samples achieve the highest roundness due to cumulative wave and eolian reworking (Fig. 18) (see also McBride and Picard, 1987; Picard and McBride, 1993; McMaster et al., 2010; Dott, 2003; Garzanti et al., 2015 a,b).

Linking inland to offshore, the modern Tiber system defines three end-member petrofacies from river to shelf. River sands span lithic to feldspatho-litho-quartzose fields and reveal a compositional break at the Corbara Dam: above the dam, multistage recycling of Miocene turbidites dominates with common siliciclastic and carbonate lithics; below, carbonate and volcaniclastic rock fragments from Mesozoic successions and the Roman Magmatic Province increase, and the Nera (carbonate) and Aniene (volcaniclastic) tributaries drive a downstream decline in mineralogical maturity (MI=Qt/[Qt+F+Lt]) (Garzanti, 2017; Garzanti et al., 2002). On the coast, foreshore sands become quartz- and pyroxene-rich under eolian/marine winnowing, while shoreface sands are feldspar- and volcanic-lithic-rich due to hydraulic concentration in lower-energy settings and partial sheltering from dune reworking (Bellotti et al., 1994; Garzanti et al., 2002). Grain-size belts parallel to the shore-from coarse/medium in the foreshore and shallow shoreface to fine/very fine beyond ~5 m depth-map directly onto compositional zonation and mixing among dune, soil, and fluvial populations (Bellotti et al., 1993; Bellotti and Tortora, 1996; Zaghloul et al., 2009; Reddad et al., 2016; Parra et al., 2012; Bender-Whitaker et al., 2018). On the shelf and slope, intrabasinal carbonate allochems dominate nearly to exhaustion of extrabasinal fractions, especially in TC7-TC8, whereas TC6 in an incised gully retains higher noncarbonate extrabasinal grains and micas, reflecting focused riverine influence and the hydraulic concentration of platy grains in distal, lower-energy settings (Di Bella et al., 2013).

Comparison with deep-marine Pleistocene sands at ODP Site 974 refines the source-to-sink routing picture (Fig. 17). QFL and QmKP fields resemble modern Tiber shoreface and fluvial compositions, but the Site 974 lithic suite lacks the sedimentary lithics that typify the present coastal system, implying selective abrasion during long submarine transport or climatic overprinting in the source (Marsaglia et al., 1999). Volcaniclastic intervals at Site 974 record high-K tephra from the Tuscan-Roman-Campanian provinces (McCoy and Cornell, 1990), while metamorphic lithics likely arrived from eastern Sardinia via canyon-to-basin pathways feeding the Vavilov Basin (Gamberi and Marani, 2009; Gamberi et al., 2009). We infer that Pleistocene basin-plain deposition at Site 974

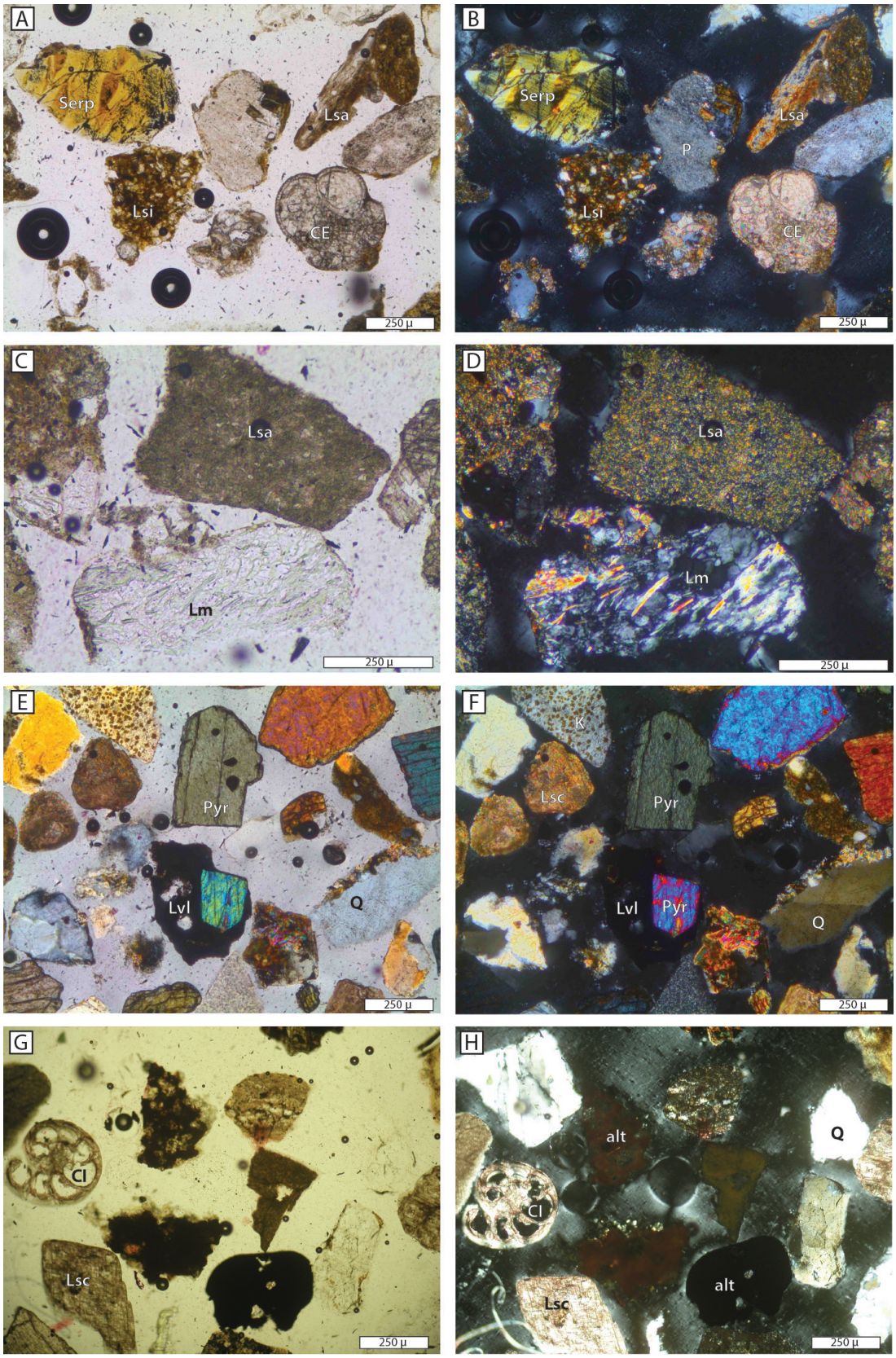

Fig. 16 - Photomicrographs illustrating representative grain types in Tiber System sands. A-B) Upstream basin sample containing serpentine (Serp), plagioclase (P), extrabasinal carbonate bioclasts (CE), and lithic fragments of claystone (Lsa) and siltstone (Lsi). C-D) Middle basin sample with claystone (Lsa) and metamorphic (Lm) lithic fragments. E-F) Lower basin sample showing quartz (Q), pyroxene (Pyr), K-feldspar (K), carbonate (Lsc) and volcanic (Lvl) lithic fragments. G-H) Coastal sample near the Tiber River mouth containing intrabasinal carbonate bioclasts (CI), alterites (alt), and carbonate lithic fragments. Each pair shows plane-polarized light on the left and cross-polarized light on the right (from Tentori et al., 2018).

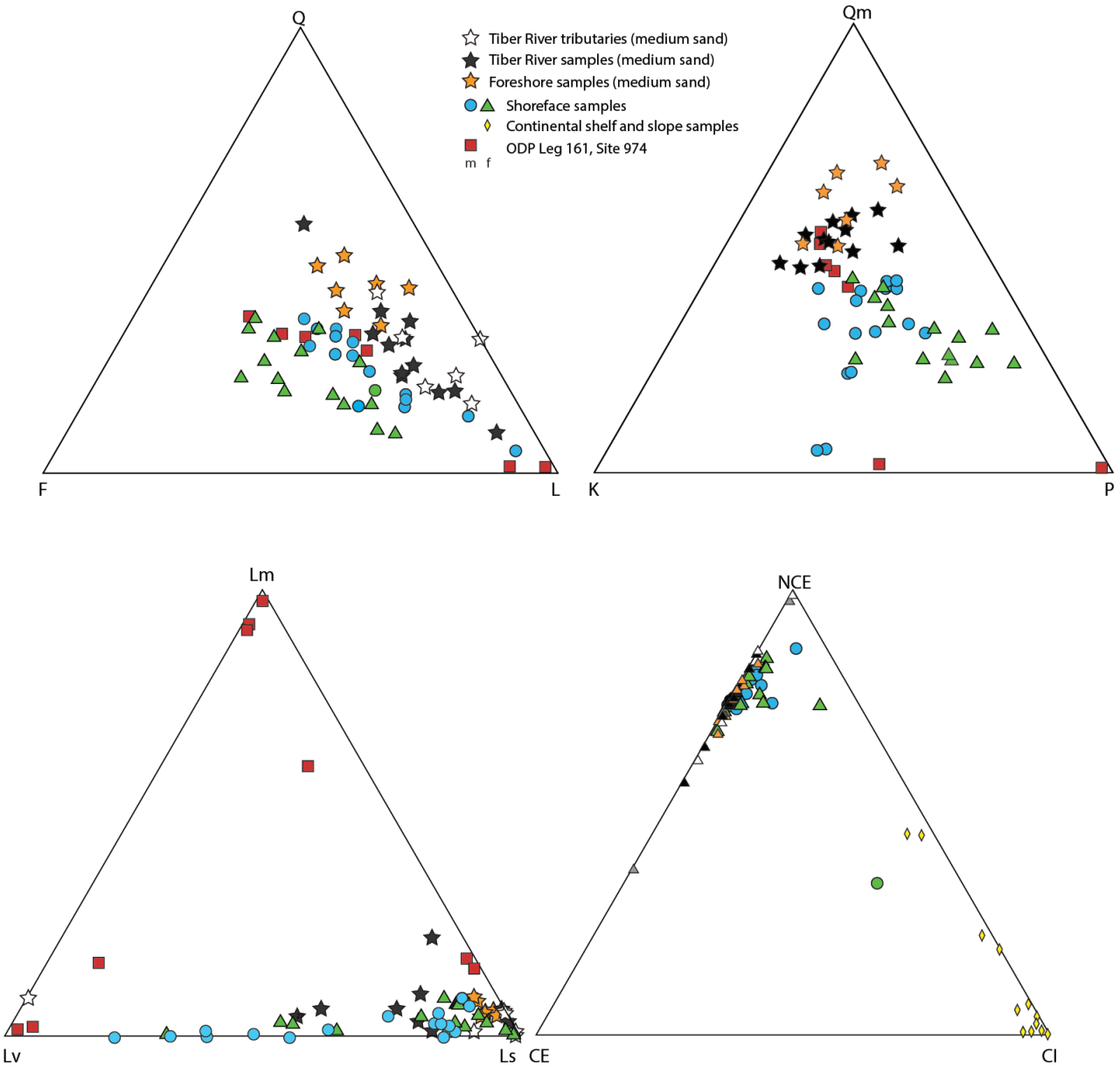

Fig. 17 - QFL, QmKP, LmLvLs, and NCE–CE–CI ternary plots for fluvial, coastal (m = medium-grained sand; f = fine-grained sand), and continental shelf to slope petrofacies of the TDS, based on ODP Leg 161, Site 974 data (Marsaglia et al., 1999) (from Tentori et al., 2018).

preferentially coincided with relative lowstands, when river mouths connected efficiently to slope conduits and multiple volcanic sources were active, whereas during the present highstand Tiber sand is largely trapped on the coast and inner shelf.

Finally, modern anthropogenic modification complicates source-sink connectivity and the provenance signal. The Corbara Dam, built in the 1950s, partitioned the Tiber into two hydrographic sub-basins, reduced sediment discharge, and shifted the coastal sand signature to reflect primarily the Paglia plus lower-Tiber reach, a pattern evident in the clustering of river and marine samples (Fig. 19). More broadly, dams and natural lakes sequester upland detritus, producing counterintuitive petrofacies in downstream tributaries and emphasizing that, in many modern deltas, the effective "sources" of marine sand are the lower drainage basins rather than the entire catchment (Syvitski and Milliman, 2007; Syvitski et al., 2005; Romans et al., 2016). These observations underscore a central implication of this study: stratigraphic stacking patterns and sand petrography may record different aspects of the same forcing history-uplift and eustasy dominating architecture, volcanism and reworking dominating composition-and misclassification of coeval versus non-coeval volcanic grains can blur interpretations of volcanic forcing versus recycled source changes. Integrating petrofacies with texture, grain-size partitioning, and independent chronostratigraphy provides a practical pathway to separate allogenic from autogenic signals in both Quaternary and ancient successions.

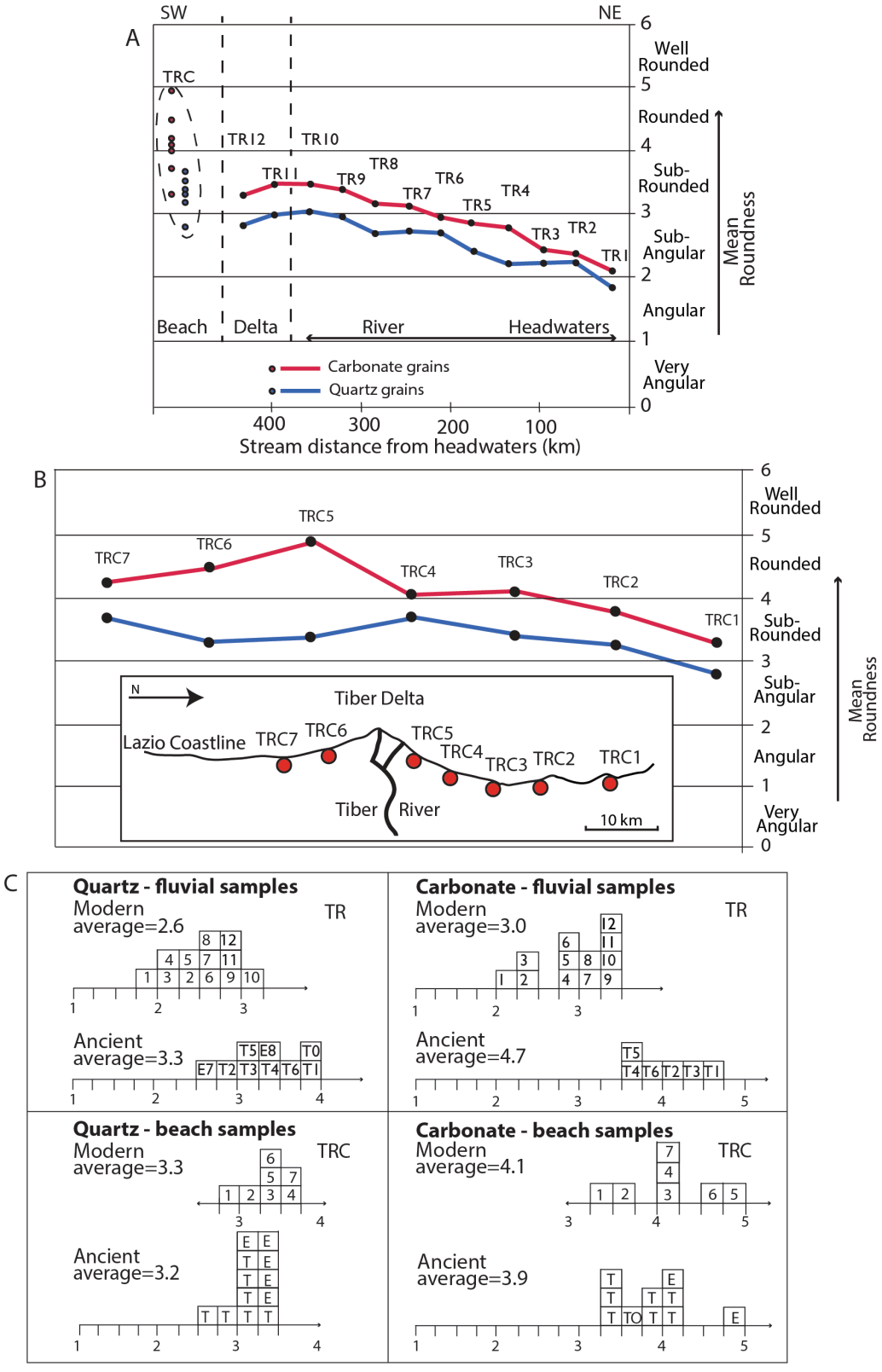

Fig. 18 - A) Variation in mean roundness of Tiber River fluvial sand from headwaters to lower reaches, showing an overall downstream increase for both quartz and carbonate grains. Ranges for TRC beach samples (detailed in B) are included for comparison. B) Roundness of beach sands along the Latium coast, with the highest values near the river mouth (TRC5), where wave reworking is likely strongest. The grey arrow indicates the dominant direction of alongshore drift (after Bellotti et al., 1993). C) Histogram comparing the mean roundness of quartz and carbonate grains from modern and ancient fluvial and beach deposits. Ancient fluvial quartz is rounder than its modern counterpart, and ancient fluvial carbonates are consistently rounder than modern ones. Quartz roundness in ancient and modern beach samples is similar in both range and mean, whereas carbonate grains in beach settings show a wider roundness range than quartz (from Tentori et al., 2016).

6. CONCLUSIONS

Tectonism, volcaniclastic input, and sea-level variations were the dominant allogenic controls on the sequence-stratigraphic evolution of the Latium Tyrrhenian extensional margin, with their combined effects recorded in the sand composition of both high-rank and low-rank depositional sequences of the Ponte Galeria Sequence (PGS) and in the modern Tiber River system. These drivers, however, acted in concert with autogenic processes-sediment mixing, reworking, and facies-related textural variability-that often mask or modify primary provenance signals. Interpreting compositional trends is, therefore, most straightforward when considering high-rank sequences spanning long time intervals (~1 Ma), where the signal-to-noise ratio of allogenic processes is higher. In contrast, the shorter duration and higher preservation potential of low-rank sequences (<100 ka) result in greater facies heterogeneity and superposition of local processes, complicating the separation of time-dependent signals from depositional overprints.

In the PGS, volcanic activity exerted a particularly strong control, dividing the succession into pre-volcanic, syn-volcanic, and post-volcanic phases. Explosive eruptions during the syn-volcanic interval supplied abundant juvenile detritus directly to fluvial, coastal, and deltaic environments, dramatically altering petrofacies and mineral proportions. Post-volcanic tectonic uplift reorganized the drainage network, altered sediment supply, and maintained a strong influence over compositional trends, often overriding the effects of glacio-eustatic fluctuations.

The modern Tiber River system detrital modes show fluvial sand composition reflecting mixing of siliciclastic (~50-70%), carbonate (~10-30%), and volcanic (~15%) source lithologies, with marked petrofacies contrasts between the upper basin-dominated by siliciclastic sedimentary lithics from Miocene foredeep turbidites-and the lower basin, where carbonate and volcanic lithics are more abundant. Hydraulic sorting and reworking of coastal dune sand and paleosol-derived volcaniclastic debris further modify compositions in the coastal zone: foreshore sands are enriched in well-sorted monomineralic quartz and pyroxene, whereas shoreface deposits are richer in feldspar and volcanic lithics hydraulically concentrated by alongshore currents. On the continental shelf and slope, modern sediments are overwhelmingly intrabasinal carbonate bioclasts, with extrabasinal signatures limited to sporadic river-influenced events or bypass via incised gullies.

Comparison with Pleistocene deep-marine sands at ODP Site 974 reveals marked differences from modern river and coastal petrofacies, implying multiple sources and different dispersal pathways under varying volcanic, tectonic, and sea-level conditions. These differences underscore the importance of recognizing that autogenic processes-especially in highstand conditions-can dominate compositional patterns even when the stratigraphic architecture is strongly influenced by allogenic forcing.

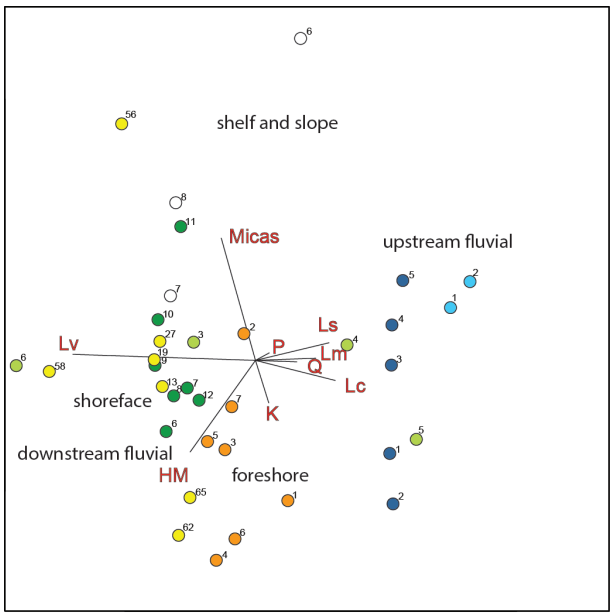

Fig. 19 - This compositional biplot (Gabriel, 1971) displays both data (samples) and parameters (rays; Q, total quartz; K, K-feldspar; P, plag; Lc, carbonate lithics; Lm, metamorphic lithics; Lv, volcanics; Hm, dense minerals). The length of each ray is proportional to the variability of the parameter in the dataset; the angle between two rays reveals whether the corresponding parameters are well correlated (0°), uncorrelated (90°), or inversely correlated (180°) (from Veermesch et al., 2016). Note that downstream fluvial samples cluster with marine sand (from Tentori et al., 2018).

From both the ancient and modern systems, a key implication is that petrofacies can be linked directly to depositional environments and systems tracts, enabling the prediction of lithological and textural properties away from control points. This has both scientific and applied significance, as compositional and textural data underpin reservoir and aquifer characterization. However, the study also highlights the limitations of using petrography in isolation to determine sequence-stratigraphic architecture, especially where multiple forcing mechanisms operate simultaneously or where unconformities are not associated with clear compositional shifts.

Ultimately, a robust interpretation of sediment compositional trends requires integrating qualitative petrographic analysis with quantitative sediment budget estimates and coupling provenance studies with detailed knowledge of catchment geology, geomorphology, climate, and depositional processes. Modern analogs such as the Tiber River system provide critical calibration for ancient successions, helping to identify environmental biases and post-depositional alterations that can obscure primary provenance signals.

ACKNOWLEDGEMENTS - This review paper aims to highlight the importance of sedimentary petrography in contributing to better defining the sequence-stratigraphic framework of the sedimentary successions, in particular in cases where a well-defined stratigraphic scheme is lacking. We thank the two anonymous referees for reviewing and providing critical comments that improved the manuscript. Funds for this research were supported by MUR (Ministero dell'Università e della Ricerca), SAPIENZA University of Rome, CNR (Consiglio Nazionale delle Ricerche), CARG Project-Geological Map of Italy 1:50,000, and Autorità Portuale di Civitavecchia, Fiumicino e Gaeta.

REFERENCES

Allen P.A., 2017. Sediment routing systems: The fate of sediment from source to sink. Cambridge University Press.

Amendola U., Perri F., Critelli S., Monaco P., Cirilli S., Trecci T., Rettori R., 2016. Composition and provenance of the Macigno Formation (Late Oligocene-Early Miocene) in the Trasimeno Lake area (Northern Apennines). Marine and Petroleum Geology 69, 146-167.

Amorosi A., 1995. Glaucony and sequence stratigraphy: a conceptual framework of distribution in siliciclastic sequences. Journal of Sedimentary Research 65, 419-425.

Amorosi A., Zuffa G.G., 2011. Sand composition changes across key boundaries of siliciclastic and hybrid depositional sequences. Sedimentary Geology 236, 153-163.

Amorosi A., Maselli V., Trincardi F., 2016. Onshore to offshore anatomy of a late Quaternary source-to-sink system (Po Plain-Adriatic Sea, Italy). Earth-Science Reviews 153, 212-237.

Barberi F., Buonasorte G., Cioni R., Fiordelisi A., Foresi L., Iaccarino S., Laurenzi M.A., Sbrana A., Vernia L., Villa I.M., 1994. Plio-Pleistocene geological evolution of the geothermal area of Tuscany and Lazio. Memorie Descrittive della Carta Geologica d'Italia 49, 77-134.

Basu A., Bickford M.E., Patranabis-Deb S., Dhang P.C., 2009. $^{207}Pb/^{206}Pb$ SHRIMP ages of detrital zircons in the Mesoproterozoic Chhattisgarh Basin, Central India, aid in identifying relative low-stand and high-stand sandstones. Geological Society of America, Annual Meeting, Portland, 18-21 October 2009.

Bellotti P., Chiocci F.L., Milli S., Tortora P., 1993. Variabilità nel tempo della distribuzione granulometrica sui fondali del delta del Tevere. Bollettino della Società Geologica Italiana 112, 143-153.

Bellotti P., Chiocci F.L., Milli S., Tortora P., Valeri P., 1994. Sequence stratigraphy and depositional setting of the Tiber delta: integration of high-resolution seismics, well logs, and archeological data. Journal of Sedimentary Research 64, 416-432.

Bellotti P., Tortora P., 1996. I sedimenti sul fondale del delta del Fiume Tevere. Bollettino della Società Geologica Italiana 115, 449-458.

Bender-Whitaker C., Marsaglia K.M., Browne G.H., Jaeger J.M., 2018. Sedimentary processes and sequence stratigraphy of a Quaternary siliciclastic shelf–slope system: insights from sand provenance studies, Canterbury Basin, New Zealand. In: Ingersoll R.V., Lawton T.F., Graham S.A. (Eds.), Tectonics, Sedimentary Basins, and Provenance: A Celebration of the Career of William R. Dickinson. Geological Society of America, Special Paper 540, 159-196.

Bordoni P., Valensise G., 1998. Deformation of the 125 ka marine terrace in Italy: tectonic implications. In: Stewart, I.S., Finzi, C.V. (Eds.), Coastal Tectonics. Geological Society of London, Special Publication 146, 71-110.

Borrelli L., Perri F., Critelli S., Gullà G., 2012. Minero-petrographical features of weathering profiles in Calabria, southern Italy. Catena 92, 196-207.

Cameron K.L., Blatt H., 1971. Durabilities of sand size schist and "volcanic" rock fragments during fluvial transport, Elk Creek, Black Hills, South Dakota. Journal of Sedimentary Petrology 41, 565-576.

Castorina F., Masi U., Milli S., Anzidei A.P., Bulgarelli G.M., 2015. Geochemical and Sr-Nd isotopic characterization of Middle Pleistocene sediments from the paleontological site of La Polledrara di Cecanibbio (Sabatini Volcanic District, central Italy). Quaternary International 357, 253-263.

Catuneanu O., Galloway W.E., Kendall C.G.St .C., Miall A.D., Posamentier H.W., Strasser A., Tucker M.E., 2011. Sequence stratigraphy: methodology and nomenclature. Newsletters on Stratigraphy 44, 173-245.

Cavinato G., De Rita D., Milli S., Zarlenga F., 1992. Correlazione tra i principali eventi tettonici, sedimentari, vulcanici ed eustatici che hanno interessato l'entroterra (conche intrappenniniche) ed il margine costiero tirrenico laziale durante il Pliocene superiore ed il Pleistocene. Studi Geologici Camerti, Volume Speciale 1992/1, 109-114.

Cioni R., Laurenzi M.A., Sbrana A., Villa I.M., 1993. $^{40}Ar/^{39}Ar$ chronostratigraphy of the initial activity in the Sabatini Volcanic Complex (Italy). Bollettino della Società Geologica Italiana 112, 251-263.

Conticelli S., Peccerillo A., 2002. Petrology and geochemistry of potassic and ultrapotassic volcanism in central Italy: petrogenesis and inferences on the evolution of the mantle sources. Lithos 28, 221-240.

Covault J.A., Craddock W.H., Romans B.W., Fildani A., Gosai M., 2013. Spatial and temporal variations in landscape evolution: historic and longer-term sediment flux through global catchments. The Journal of Geology 121, 35-56.

Critelli S., Le Pera E., 1994. Detrital modes and provenance of Miocene sandstones and modern sands of the southern Apennines thrust-top basins (Italy). Journal of Sedimentary Research 64, 824-835.

Critelli S., Le Pera E., 2002. Provenance relations and modern sand petrofacies in an uplifted thrust-belt, northern Calabria, Italy. In: Basu A., Vallone R. (Eds.), Quantitative Provenance Studies in Italy. Memorie Descrittive della Carta Geologica d'Italia 61, 25-38.

Critelli S., Le Pera E., Ingersoll R.V., 1997. The effects of source lithology, transport, deposition and sampling scale on the composition of southern California sand. Sedimentology 44, 653-671.

Crook K.A.W., 1960. Classification of arenites. American Journal of Science 258, 419-428.

De Rita D., Milli S., Rosa C., Zarlenga F., Cavinato G.P., 1994. Catastrophic eruptions and eustatic cycles: example of Lazio

volcanoes. Atti dei Convegni Lincei 112, 135-142.

De Rita D., Fabbri M., Mazzini I., Paccara P., Sposato A., Trigari A., 2002. Volcaniclastic sedimentation in coastal environments: the interplay between volcanism and Quaternary sea level changes (central Italy). Quaternary International 95-96, 141-154.

Di Bella L., Bellotti P., Milli S., 2013. The role of foraminifera as indicators of the Late Pleistocene-Holocene palaeoclimatic fluctuations on the deltaic environment: the example of Tiber delta succession (Tyrrhenian margin, Italy). Quaternary International 303, 191-209.

Dickinson W.R., 1970. Interpreting detrital modes of graywacke and arkose. Journal of Sedimentary Petrology 40, 695-707.

Dickinson W.R., 1985. Interpreting provenance relations from detrital modes of sandstones. In: Zuffa G.C. (Ed.), Provenance of Arenites. NATO ASI Series, D. Reidel Publishing Company, Dordrecht, The Netherlands, 333-362.

Doglioni C., Innocenti F., Morellato C., Procaccianti D., Scrocca D., 2004. On the Tyrrhenian Sea opening. Memorie Descrittive della Carta Geologica d'Italia 64, 147-164.

Dott R.H., 2003. The importance of eolian abrasion in supermature quartz sandstones and the paradox of weathering on vegetation free-landscapes. The Journal of Geology 111, 387-405.

Funiciello R., Locardi E., Parotto M., 1976. Lineamenti geologici dell'area sabatina orientale. Bollettino della Società Geologica Italiana 95, 831-849.

Gabriel K.R., 1971. The biplot graphic display of matrices with application to principal component analysis. Biometrika 58, 453-467.

Gamberi F., Marani M., 2009. Control of regional geology on the style of basin-plain depositional systems in the Tyrrhenian Sea. In: Kneller, B., Martinsen, O.J., McCaffrey, B. (Eds.), External Controls on Deep-Water Depositional Systems. SEPM Special Publication 92, 221-232.

Gamberi F., Dalla Valle G., Kneller B., 2009. The impact of margin-shaping processes on the architecture of the Sardinian and Sicilian margin submarine depositional systems within the Tyrrhenian Sea. In: Kneller, B., Martinsen, O.J., McCaffrey, B. (Eds.), External Controls on Deep-Water Depositional Systems. SEPM Special Publication 92, 207-219.

Gandolfi G., Paganelli L., 1993. Le torbiditi arenacee Oligo-Mioceniche dell'Apennino settentrionale fra la Spezia ed Arezzo-Studio petrografico ed implicazioni paleogeografiche: Giornale di Geologia 55, 93-102.

Gandolfi G., Paganelli L., Zuffa G.G., 1983. Petrology and dispersal pattern in the Marnoso Arenacea Formation (Miocene, Northern Apennines). Journal of Sedimentary Petrology 53, 493-507.

Gandolfi G., Paganelli L., Cavazza W., 2007. Heavy-mineral associations as tracers of limited compositional mixing during turbiditic sedimentation of the Marnoso-Arenacea Formation (Miocene, Northern Apennines, Italy). Amsterdam, Elsevier, Developments in Sedimentology 58, 621-645.

Garçon M., Chauvel C., France-Lanord C., Limonta M., Garzanti E., 2014. Which minerals control the Nd-Hf-Sr-Pb isotopic compositions of river sediments? Chemical Geology 364, 42-55.

Garzanti E., 1991. Non-carbonate intrabasinal grains in arenites: their recognition, significance and relationship to eustatic cycles and tectonic setting. Journal of Sedimentary Research 61, 959-975.

Garzanti E., 2016. From static to dynamic provenance analysis-sedimentary petrology upgraded. Sedimentary Geology 336, 3-13.

Garzanti E., 2017. The maturity myth in sedimentology and provenance analysis. Journal of Sedimentary Research 87, 353-365.

Garzanti E., Vezzoli G., 2003. A classification of metamorphic grains in sands based on their composition and grade. Journal of Sedimentary Research 73, 830-837.

Garzanti E., Andò S., Vezzoli G., 2009. Grain-size dependence of sediment composition and environmental bias in provenance studies. Earth and Planetary Science Letters 277, 422-432.

Garzanti E., Vezzoli G., Andò S., 2011. Paleogeographic and paleodrainage changes during Pleistocene glaciations (Po Plain, northern Italy). Earth-Science Reviews 105, 25-48.

Garzanti E., Canclini S., Foggia F.M., Petrella N., 2002. Unraveling magmatic and orogenic provenance in modern sand: the back-arc side of the Apennine thrust belt, Italy. Journal of Sedimentary Research 72, 2-17.

Garzanti E., Andò S., Vezzoli G., Dell'Era D., 2003. From rifted margins to foreland basins: investigating provenance and sediment dispersal across desert Arabia (Oman, U.A.E.). Journal of Sedimentary Research 73, 572-588.

Garzanti E., Resentini A., Andò S., Vezzoli G., Vermeesch P., 2015a. Physical controls on sand composition and relative durability of detrital minerals during long-distance littoral and eolian transport (coastal Namibia). Sedimentology 62, 971-996.

Garzanti E., Andò S., Padoan M., Vezzoli G., El Kammar A., 2015b. The modern Nile sediment system: processes and products. Quaternary Science Reviews 130, 9-56.

Garzanti E., Padoan M., Andò S., Resentini A., Vezzoli G., Lustrino M., 2013. Weathering and relative durability of detrital minerals in equatorial climate: sand petrology and geochemistry in the East African Rift. The Journal of Geology 121, 547-580.

Giordano G., Esposito A., De Rita D., Fabbri M., Mazzini I., Trigari A., Rosa C., Funiciello R., 2003. The sedimentation along the Roman coast between Middle and Upper Pleistocene: the interplay of eustatism, tectonics and volcanism-new data and review. Il Quaternario 16, 121-129.

Ingersoll R.V., 1983. Petrofacies and provenance of late Mesozoic forearc basin, northern and central California. American Association of Petroleum Geologists Bulletin 67, 1125-1142.

Ingersoll R.V., Bullard T.F., Ford R.L., Grimm J.P., Pickle J.D., Sares S.W., 1984. The effect of grain size on detrital modes: a test of the Gazzi-Dickinson point counting method. Journal of Sedimentary Petrology 54, 103-116.

Ito M., 1991. Compositional variation in depositional sequences of the upper part of the Kasuza Group, a middle Pleistocene forearc basin fill in the Boso Peninsula, Japan. Sedimentary Geology 88, 219-230.

Ito M., 1994. Compositional variation in depositional sequences

of the upper part of the Kasuza Group, a middle Pleistocene forearc basin fill in the Boso Peninsula, Japan. Sedimentary Geology 88, 219-230.

James D.E., Devaughn A.M., Marsaglia K.M., 2007. Sand and gravel provenance in the Waipaoa River System: sedimentary recycling in an actively deforming forearc basin, North Island, New Zealand. In: Arribas J., Critelli, S., Johnsson, M. (Eds.), Sedimentary Provenance: Petrographic and Geochemical Perspectives. Geological Society of America, Special Paper 420, 253-276.

Johnsson M.J., 1990. Overlooked sedimentary particles from tropical weathering environments. Geology 18, 107-110.

Karner D.B., Marra F., Renne P.R., 2001. The history of the Monti Sabatini and Alban Hills volcanoes: groundwork for assessing volcanic-tectonic hazards for Rome. Journal of Volcanology and Geothermal Research 107, 185-219.

Lawton T.F., Pollock S.L., Robinson R.A.J., 2003. Integrating sandstone petrology and nonmarine sequence stratigraphy: application to the Late Cretaceous fluvial systems of southwestern Utah, U.S.A. Journal of Sedimentary Research 73, 389-406.

Leombruni A., Blois L., Mancini M., 2009. First evaluation of soil erosion and sediment delivery in the high part of the Tevere watershed. Electronic Journal of Geotechnical Engineering 14, 1-26.

Malinverno A., Ryan W.B.F., 1986. Extension in the Tyrrhenian Sea and shortening in the Apennines as result of arc migration driven by sinking of the lithosphere. Tectonics 5, 227-245.

Mancini M., Cavinato G.P., 2005. The Middle Valley of the Tiber River, central Italy: Plio-Pleistocene fluvial and coastal sedimentation, extensional tectonics and volcanism. In: Blum, M., Marriot, S., Leclair, S. (Eds.), Fluvial Sedimentology VII. International Association of Sedimentologists, Special Publication 35, 373-396.

Marchesini L., Amorosi A., Cibin U., Spadafora E., Zuffa G.G., Preti D., 2000. Detrital supply versus facies architecture in the late Quaternary deposits of the southeastern Po Plain (Italy). Journal of Sedimentary Research 70, 829-838.

Mariani M., Prato R., 1988. I bacini neogenici costieri del margine tirrenico: approccio sismo-stratigrafico. Memorie della Società Geologica Italiana 41, 519-531.

Marra F., Deocampo D., Jackson M.D., Ventura G., 2011. The Alban Hills and Monti Sabatini volcanic products used in ancient Roman masonry (Italy): an integrated stratigraphic, archeological, environmental and geochemical approach. Earth-Science Reviews 108, 115-136.

Marra F., Sottili G., Gaeta M., Giaccio B., Jicha B., Masotta M., Palladino D.M., Deocampo D.M., 2014. Major explosive activity in the Monti Sabatini Volcanic District (central Italy) over the 800-390 ka interval: geochronological-geochemical overview and tephrostratigraphic implications. Quaternary Science Reviews 94, 74-101.

Marsaglia K.M., 1992. Petrography and provenance of volcaniclastic sands recovered from the Izu-Bonin Arc, Leg 126. Proceedings of the Ocean Drilling Program, Scientific Results 126, 139-154.

Marsaglia K.M., Tazaki K., 1992. Diagenetic trends in ODP Leg 126 sandstone. Proceedings of the Ocean Drilling Program, Scientific Results 126, 125-138.

Marsaglia K.M., Latter K.K., Cline V., 1999. Sand provenance in the Alboran and Tyrrhenian basins. Proceedings of the Ocean Drilling Program, Scientific Results 161, 37-56.

Marsaglia K.M., DeVaughn A.M., James D.E., Marden M., 2010. Provenance of fluvial terrace sediments within the Waipaoa sedimentary system and their importance to New Zealand source-to-sink studies. Marine Geology 270, 84-93.

McBride E.F., 1985. Diagenetic processes that affect provenance determination in sandstone. In: Zuffa, G.G. (Ed.), Provenance of Arenites. NATO ASI Series, Dordrecht, Reidel, 95-114.

McBride E.F., Picard M.D., 1987. Downstream changes in sand composition, roundness, and gravel size in a short-headed, high-gradient stream, northwestern Italy. Journal of Sedimentary Petrology 57, 1018-1026.

McCoy F.W., Cornell W., 1990. Volcaniclastic sediments in the Tyrrhenian Basin. Proceedings of the Ocean Drilling Program, Scientific Results 107, 291-305.

Mcmaster K., Whitmore J.H., Strom R., 2010. A comparison of beach and dune sands along the southern Oregon coast, USA. Geological Society of America, Abstracts with Programs 42, 311-322.

Milli S., 1997. Depositional setting and high-frequency sequence stratigraphy of the Middle-Upper Pleistocene to Holocene deposits of the Roman Basin. Geologica Romana 33, 99-136.

Milli S., 1994. High-frequency sequence stratigraphy of the Middle-Upper Pleistocene to Holocene deposits of the Roman Basin (Rome, Italy): relationships among high-frequency eustatic cycles, tectonics and volcanism. In: Posamentier H.W., Mutti E. (Eds.), Second High-Resolution Sequence Stratigraphy Conference. Tremp, Spain, 20-27 June.

Milli S., Moscatelli M., 2001. The Torre in Pietra section: sedimentology and physical stratigraphy. Poster session, 1st International Congress, The World of Elephants, Rome, 16-20 October.

Milli S., Moscatelli M., Palombo M.R., Parlagreco L., Paciucci M., 2008. Incised valleys, their filling and mammal fossil record: a case study from Middle–Upper Pleistocene deposits of the Roman Basin (Latium, Italy). In: Amorosi A., Haq B.U., Sabato L. (Eds.), Advances in Application of Sequence Stratigraphy in Italy. GeoActa Special Publication 1, 67-87.

Milli S., D'Ambrogi C., Bellotti P., Calderoni G., Carboni M.G., Celant A., Di Bella L., Di Rita F., Frezza V., Magri D., Pichezzi R.M., Ricci V., 2013. The transition from wave-dominated estuary to wave-dominated delta: the Late Quaternary stratigraphic architecture of Tiber River deltaic succession (Italy). Sedimentary Geology 284-285, 159-180.

Milli S., Mancini M., Moscatelli M., Stigliano F., Marini M., Cavinato G.P., 2016. From river to shelf, anatomy of a high-frequency depositional sequence: the Late Pleistocene to Holocene Tiber depositional sequence. Sedimentology 63, 1886-1928.

Mitchum R.M. Jr., Van Wagoner J.C., 1991. High-frequency sequences and their stacking pattern: sequence stratigraphic evidence of high-frequency eustatic cycles. Sedimentary Geology 70, 131-170.

Nesbitt H.W., Young G.M., 1996. Petrogenesis of sediments in the absence of chemical weathering: effects of abrasion and

sorting on bulk composition and mineralogy. Sedimentology 42, 341-358.

Parra J.G., Marsaglia K.M., Rivera K.S., Dawson S.T., Walsh J.P., 2012. Provenance of sand on the Poverty Bay shelf, the link between source and sink sectors of the Waipaoa River sedimentary system. Sedimentary Geology 280, 208-233.

Patacca E., Sartori R., Scandone P., 1990. Tyrrhenian basin and Apenninic arc: kinematic relations since late Tortonian times. Memorie della Società Geologica d'Italia 45, 425-451.

Peccerillo A., 2005. Plio-Quaternary volcanism in Italy: petrology, geochemistry, geodynamics. Springer, Heidelberg, p. 365.

Picard M.D., Mcbride E.F., 1993. Beach sands of Elba Island, Tuscany, Italy: Roundness study and evidence of provenance. In: Johnsson M.J., Basu A. (Eds.), Processes Controlling the Composition of Clastic Sediments. Geological Society of America, Special Paper 284, 235-246.

Posamentier H.W., Allen G.P., 1999. Siliciclastic Sequence Stratigraphy-Concepts and Applications. SEPM Concepts in Sedimentology and Paleontology, 7, 210.

Reddad H., El Talibi H., Perri F., El Moussaoui S., Zerdeb M.A., Zaghloul M.N., Critelli S., 2016. Textural and compositional controls on modern fluvial and beach sands of Mediterranean coastal Rif belt (Northern Rif, Morocco). Italian Journal of Geosciences 135, 336-349.

Romans B.W., Castelltort S., Covault J.A., Fildani A., Walsh J.P., 2016. Environmental signal propagation in sedimentary systems across timescales. Earth-Science Reviews 153, 7-29.

Sottili G., Palladino D.M., Marra F., Jicha B., Karner D.B., Renne P., 2010. Geochronology of the most recent activity in the Sabatini Volcanic District, Roman Province, central Italy. Journal of Volcanology and Geothermal Research 196, 20-30.

Stalder N.F., Fellin M.G., Caracciolo L., Guillong M., Winkler W., Milli S., Moscatelli M., Critelli S., 2018. Dispersal pathways in the early Messinian Adriatic foreland and provenance of the Laga Formation (Central Apennines, Italy). Sedimentary Geology 375, 289-308.

Syvitski J.P., Milliman J.D., 2007. Geology, geography, and humans battle for dominance over the delivery of fluvial sediment to the coastal ocean. The Journal of Geology 115, 1-19.

Syvitski J.P.M., Vörösmarty C.J., Kettner A.J., Green P., 2005. Impact of humans on the flux of terrestrial sediment to the global coastal ocean. Science 308, 376-380.

Tentori D., Marsaglia K.M., Milli S., 2016. Sand compositional changes as a support for sequence-stratigraphic interpretation: the Middle-Upper Pleistocene to Holocene deposits of the Roman Basin (Rome, Italy). Journal of Sedimentary Research 86, 1208-1227.

Tentori D., Milli S., Marsaglia K.M., 2018. A source-to-sink compositional model of a present highstand: an example in the low-rank Tiber depositional sequence (Latium Tyrrhenian margin, Italy). Journal of Sedimentary Research 88, 1238-1259.

Tentori D., Amorosi A., Milli S., Marsaglia K.M., 2021. Sediment dispersal pathways in the Po coastal plain since the Last Glacial Maximum: Provenance signals of autogenic and eustatic forcing. Basin Research 33, 1407-1428.

Tentori D., Mancini M., Milli S., Stigliano F., Tancredi S., Moscatelli M., 2022. Compositional, micromorphological and geotechnical characterization of Holocene Tiber floodplain deposits (Rome, Italy) and sequence stratigraphic implications. Sedimentology 69, 1705-1737.

Tentori D., Mancini M., Stigliano F., Milli S., Simionato M., Livani M., Moscatelli M., 2025. Integrating sequence stratigraphy and geostatistical methods for 3D lithofacies modelling of the Tiber alluvial plain, Rome, Italy. Basin Research 37, e70024.

Tomassi A., Milli S., Tentori D., 2024. Synthetic seismic forward modeling of a high-frequency depositional sequence: The example of the Tiber depositional sequence (Central Italy). Marine and Petroleum Geology 160, 106624.

Valloni V., Zuffa G.G., 1984. Provenance changes for arenaceous formations of the northern Apennines, Italy. Geological Society of America Bulletin 95, 1035-1039.

Veermesch P., Resentini A., Garzanti E., 2016. An R package for statistical provenance analysis: Sedimentary Geology 336, 14-25.

Villaseñor T., Tentori D., Marsaglia K.M., Pinto, L., 2020. The changing Patagonian landscape: Erosion and westward sediment transfer paths in northern Patagonia during the Middle and Late Pleistocene. Basin Research 32, 1035-1053.

Weltje G.J., 2006. Ternary sandstone composition and provenance: an evaluation of the "Dickinson model." In: Buccianti, A., Mateu-Figueras, G., Pawlowsky-Glahn, V. (Eds.), Compositional Data Analysis: From Theory to Practice. Geological Society of London, Special Publication 264, 611-627.

Young S.W., Basu A., Mack G., Darnell H., Suttner L.J., 1975. Use of size-composition trends in Holocene soil and fluvial sand for paleoclimatic interpretation. Proceedings IXth International Congress of Sedimentology, Nice, France, 28-36.

Zaghloul M.N., Reddad H., Critelli S., 2009. Source-area controls on the composition of beach and fluvial sands on the southern side of the Gibraltar Strait and western Alboran Sea (Flysch Basin, Internal and External Domains, Northern Rif Chain). Journal of African Earth Sciences 55, 36-46.

Zuffa G.G., 1980. Hybrid arenites: their composition and classification. Journal of Sedimentary Petrology 50, 21-29.

Zuffa G.G., 1985. Optical analyses of arenites: influence of methodology on compositional results. In: Zuffa, G.G. (Ed.), Provenance of Arenites. NATO-ASI, Dordrecht, Reidel, 165-189.

Zuffa G.G., 1987. Unravelling hinterland and offshore palaeogeography from deep-water arenite. In: Leggett, J.K., Zuffa, G.G. (Eds.), Marine Clastic Sedimentology: Models and Case Studies. Graham and Trotman, London, 39-61.

Zuffa G.G., 1991. On the use of turbidite arenites in provenance studies: critical remarks. In: Morton A.C., Todd S.P., Haughton P.D.W. (Eds.), Developments in Sedimentary Provenance Studies. Geological Society of London, Special Publication 57, 21-28.

Zuffa G.G., Cibin U., Di Giulio A., 1995. Arenite petrography in sequence stratigraphy. Journal of Geology 103, 451-459.